STUDY OF NEUTRINO INTERACTIONS IN THE CHORUS EXPERIMENT

A THESIS SUBMITTED TO
THE GRADUATE SCHOOL OF NATURAL AND APPLIED SCIENCES
OF
MIDDLE EAST TECHNICAL UNIVERSITY

BY

VOLKAN ÇUHA

IN PARTIAL FULFILLMENT OF THE REQUIREMENTS

FOR

THE DEGREE OF MASTER OF SCIENCE

IN

PHYSICS

NOVEMBER 2006

Approval of the Graduate School of Natural and Applied Sciences.

Prof. Dr. Canan Özgen
Director

I certify that this thesis satisfies all the requirements as a thesis for the degree of Master of Science.

Prof. Dr. Sinan Bilikmen
Head of Department

This is to certify that we have read this thesis and that in our opinion it is fully adequate, in scope and quality, as a thesis for the degree of Master of Science.

Assoc. Prof. Dr. Ali Murat Güler
Supervisor

Examining Committee Members

Prof. Dr. Ramazan SEVER (METU,PHYS) _____

Assoc. Prof. Dr. Ali Murat GÜLER (METU,PHYS) _____

Prof. Dr. Gürsevil TURAN (METU,PHYS) _____

Assist. Prof. Dr. Osamu SATO (Nagoya Uni.,PHYS) _____

Prof. Dr. Satılmış ATAĞ (Ankara Uni.,PHYS) _____

"I hereby declare that all information in this document has been obtained and presented in accordance with academic rules and ethical conduct. I also declare that, as required by these rules and conduct, I have fully cited and referenced all material and results that are not original to this work."

Name Surname : VOLKAN ÇUHA

Signature :

ABSTRACT

STUDY OF NEUTRINO INTERACTIONS IN THE CHORUS EXPERIMENT

VOLKAN, ÇUHA

M.S., Department of Physics

Supervisor: Assoc. Prof. Dr. Ali Murat Güler

November 2006, 72 pages.

The emulsion target of the CHORUS detector was exposed to the wide-band neutrino beam of the CERN SPS between the years 1994 and 1997. In total about 130.000 neutrino interactions were located in the nuclear emulsion target and fully reconstructed. Detailed DATA and Monte Carlo (MC) comparisons were done in order to test reliability of the detector simulation. There is reasonable agreement between DATA and MC. The ratio of deep inelastic neutral-current (NC) to the deep inelastic (DIS) charged-current(CC) ν_μ interactions was measured to be $\frac{NC_{dis}}{CC_{dis}} = 0.350 \pm 0.003$. This measurement was compared with the previous measurements. Based on three double charm decays found in NC interactions we measured the ratio of double charm cross-section in NC ν_μ interactions to be

$$\frac{\sigma(c\bar{c}\nu_\mu)}{\sigma_{NC}} = (3.37^{+3.06}_{-2.51}(stat.) \pm 0.51(syst.)) \times 10^{-3}.$$

One double charm decay has been observed in CC ν_μ interactions the upper limit on associated charm production in ν_μ CC interaction has been found to be

$$\frac{\sigma(c\bar{c}\mu^-)}{\sigma_{CC}} < 9.69 \times 10^{-4}.$$

at 90% C.L.

Keywords: Neutrino, Neutrino interaction, Monte-Carlo Data comparison, Double charm production rates

ÖZ

CHORUS DENEYİNDE NÖTRİNO ETKİLEŞİMLERİNİN İNCELENMESİ

VOLKAN, ÇUHA

Yüksek Lisans , Fizik Bölümü

Tez Yöneticisi: Doç. Dr. Ali Murat Güler

Kasım 2006, 72 sayfa.

Emülsiyon hedeften oluşan CHORUS dedektörü 1994 - 1997 yılları arasında CERN SPS'te geniş-bant nötrino hüzmesi ile bombardıman edilmiştir. Toplam 130.000 nötrino etkileşimi kaydedilmiş ve nükleer emülsiyon içinde bulunmuştur. Detaylı DATA ve Monte Carlo (MC) kıyaslamaları dedektör simülasyonlarının gerçekliliğini denemek için yapılmıştır. DATA ve MC arasında uyumlu bir ilişki vardır. DIS yüksüz zayıf etkileşimlerinin DIS yüklü etkileşimlerine oranı $\frac{NC}{CC} = 0.35 \pm 0.001$ olarak ölçülmüştür. Bu ölçüm önceki deneylerle karşlaştırılmıştır. Yüksüz zayıf etkileşiminde bulunan 3 adet çiftli charm bozunumu baz alınarak yüksüz zayıf ν_μ etkileşimindeki çiftli charm üretimi aşağıdaki gibi ölçülmüştür,
$\frac{\sigma(c\bar{c}\nu_\mu)}{\sigma_{NC}} = (3.37^{+3.06}_{-2.51}(stat.) \pm 0.51(syst.)) \times 10^{-3}$.
Yüklü zayıf ν_μ etkileşiminde bir adet çiftli charm bozunumu gözlenmiş olup, yüklü zayıf ν_μ etkileşimindeki çiftli charm üretim üst limiti %90 güvenilirlikte $\frac{\sigma(c\bar{c}\mu^-)}{\sigma_{CC}} < 9.69 \times 10^{-4}$ olarak hesaplanmıştır.

Anahtar Kelimeler: Nötrino, Nötrino etkileşimi, Monte-Carlo Data karşılaştırması, Çiftlenimli charm üretim oranı,

To my first major teacher of life, to my parents.With love and gratitude.

ACKNOWLEDGMENTS

The work presented in this thesis would not have been possible without the involvement of a number of people. I would like to thank the following persons in particular:

I would like to express my deepest gratitude to my supervisor Assoc.Prof. Dr. Ali Murat GÜLER for his help, attitude, encouragement, guidance and insight throughout this research.

There are no words to describe the appreciation and gratitude I feel for my family. I thank them for their optimism, beautiful spirits and belief in me.

I would like to express my sincere gratitude to Umut KÖSE for his invaluable help.

I would like to thank to Elif BEKLEN, Sırma ŞEN, Bülent YILMAZ and to my other friends for their help and encouragement.

TABLE OF CONTENTS

LIST OF FIGURES

LIST OF TABLES

CHAPTER 1

INTRODUCTION

Neutrinos are one of the fundamental particles which make up the universe. They are also one of the least understood.

The history of this elusive particle [1, 2] started with the discovery of radioactivity by H. Becquerel. In the years 1899 and 1900 he identified β radiation as one component of radioactivity, and demonstrated that β rays are composed of electrons. Observation of discrete energy lines in electron spectra from the decay of isotopes in the radium and thorium series was made in Berlin in the years 1910 and 1911 by von Bayer, O. Hahn, and L. Meitner [3]. This was around the same time as the experimental evidence for the atomic nucleus by E. Rutherford [4].

The continuous β spectrum was discovered in the decay of RaB (214Pb) by Chadwick [5] in 1914, using a magnetic spectrometer. Thus it was known that the electron spectra had monoenergetic lines and a continuous component, in strong contrast with α and γ ray spectra, which were known to consist of monoenergetic lines only.

Interpretation of the continuous electron spectrum was the subject of considerable debate. E. Rutherford (1914) was of the opinion that the β electrons were all emitted from the nucleus with the same energy, but lost different fractions of this energy to the surrounding atoms, depending on the source thickness traveled.

W. Pauli proposed the idea of a very penetrating neutral particle of small mass and spin-1/2, emitted with the electron in β decay. This proposal was made before Chadwick's discovery of the neutron [6] in 1932. Pauli openly proposed his hypothesis at the Solvay Congress in Brussels in 1933. E. Fermi was present, and proposed the name "neutrino" to distinguish it from the neutron. Soon afterwards, Fermi developed his famous theory of β decay [7].

In 1934, H. Bethe and R. Peierls [8] showed that the cross section between neutrinos and matter should be extremely small: billions of time smaller than the one of an electron. In order to detect such a rare process both a large target and an enormous flux was required. The first direct evidence of neutrino existence came in 1956 from an experiment performed by F. Reines and C. L. Cowan [9] at a nuclear reactor. In 1995, F. Reines was awarded the nobel prize for this discovery.

In 1962, Muon neutrinos were discovered by L. Lederman, M. Schwartz, J. Steinberger [10] and colleagues at Brookhaven National Laboratories and it was confirmed that they are different from ν_e.

In 1976, the Tau lepton was discovered by M. Perl [11] and colleagues at

SLAC in Stanford, California. After several years, analysis of Tau decay modes leads to the conclusion that Tau is accompanied by its own neutrino ν_τ which is neither ν_e nor ν_μ.

In 2000, the DONUT Collaboration [12] working at Fermilab announced observation of Tau particles produced by ν_τ, making the first direct observation of the Tau neutrino.

A massive neutrino implies physics beyond the Standard model. If the neutrinos are massive several phenomenon can occur such as mixing between different eigenstates at some distance from source. This phenomena is called neutrino oscillation which was introduced by Pontecorvo. Many experiments have been performed in order to detect neutrino oscillations. One of them is the CHORUS experiment which was designed to observe $\nu_\mu \rightarrow \nu_\tau$ oscillations. On the other hand, the CHORUS detector is also suitable for the study of charm production by neutrino interactions; because charmed hadrons have lifetimes similar to that of the Tau lepton.

The study of charm production in neutrino interactions is relevant for the determination of several quantities related to the quark physics, such as the element V_{ud} of the Cabibbo-Kobayashi-Maskawa [13, 14] matrix, the charm quark mass, strange content of the sea quarks, nucleon structure functions, the parameters entering in the quark fragmentation.

Several experiments was done in the past to investigate charm production in

neutrino interactions such as E531 [20], CDHS [21], CHARMII [22] and CCFR [23]. After the big improvement in scanning systems, the CHORUS experiment has provided high statistics for charm physics. The sub-micron resolution of the nuclear emulsion of the CHORUS detector allows an efficient search for rare processes such as the associated charm production through the observation of the double charm decay topology with a very low background. We present a search for associated charm production in ν_μ interactions based on the visual observation of two decay vertices, taking advantage of the submicrometric position resolution of the nuclear emulsions exposed in the CHORUS experiment to the CERN SPS neutrino beam.

In the following Chapter, a theoretical framework for neutrino interactions and charm production will be given. Chapter 3 describes the CHORUS detector and its features. In Chapter 4, DATA/MC comparisons and measurement of $\frac{NC}{CC}$ ratio are given. In Chapter 5, a search for associated charm production is discussed and production rates in charged and neutral current neutrino interactions are estimated.

CHAPTER 2

THEORETICAL MOTIVATION

The observed neutrino interactions are described well within the Standard Model. Neutrinos are treated as massless, neutral, left-handed particles with spin half in this model. But there is no fundamental principle stating that neutrinos must have zero mass and in fact many extensions of the Standard Model predict massive neutrinos. In the following section neutrino interaction in the framework of the Standard Model will be discussed shortly.

2.1 Neutrinos in the Standard Model

In the Sandard Model of S. Glashow [24], A. Salam [25] and S. Weinberg [26] the weak and electromagnetic interactions are introduced as different components of a single gauge theory. The standard model is based on the gauge group $SU(2)_L \mathrm{x} U(1)_Y$ generated by weak isospin and weak hypercharge. Forces are propagated through field of bosons: $W^{\pm}, Z^0$.

Both the $SU(2)_L$ and $U(1)_Y$ symmetries must be spontaneously broken. In nature, only the electromagnetic interaction and the strong interaction originate

from an unbroken symmetry. In the Standard Model gauge bosons and matter fermions acquire mass through the mechanism of spontaneous breaking of the local gauge symmetry.

The left-handed components of each generation of leptons and quarks are doublets under $SU(2)_L$ while right-handed components are singlets:

$$\begin{pmatrix} e^- \\ \nu_e \end{pmatrix}_L e^-_R, \qquad \begin{pmatrix} \mu^- \\ \nu_\mu \end{pmatrix}_L \mu^-_R, \qquad \begin{pmatrix} \tau^- \\ \nu_\tau \end{pmatrix}_L \tau^-_R \tag{2.1}$$

$$\begin{pmatrix} u \\ d' \end{pmatrix}_L u_R, d_R, \qquad \begin{pmatrix} c \\ s' \end{pmatrix}_L c_R, s_R, \qquad \begin{pmatrix} t \\ b' \end{pmatrix}_L t_R, b_R. \tag{2.2}$$

Here d', s', b' which are the weak eigenstates of the quarks are expressed as linear combination of the quark mass eigenstates via 3×3 unitary CKM (cabbibo-Kobayashi-Maskawa) [13, 14] mixing matrix given below:

$$\begin{pmatrix} d' \\ s' \\ b' \end{pmatrix} = \underbrace{\begin{pmatrix} V_{ud} & V_{us} & V_{ub} \\ V_{cd} & V_{cs} & V_{cb} \\ V_{td} & V_{ts} & V_{tb} \end{pmatrix}}_{CKM matrix} \begin{pmatrix} d \\ s \\ b \end{pmatrix} \tag{2.3}$$

In other words, the weak force does not "see" for instance a simple s quark but an s', which is a linear combination of d, s and b quarks,

$$s' = V_{cd}d + V_{cs}s + V_{cb}b. \tag{2.4}$$

The elements on the diagonal are approximately equal to one, which means that a quark most likely make a translation within its own generation. The matrix elements becomes smaller as the elements goes off the diagonal. Based on this, interactions that involve matrix elements that lie on the diagonal are considered 'Cabbibo Favored' while those that involve off-diagonal elements are said to be 'Cabbibo Suppresed'

2.2 Quantum Chromodynamics

The dynamics of quarks is described by a non-abelian gauge theory, the Quantum Chromodynamics(QCD) [15].

In strong interaction, experiments confirm that each quark has another internal degree of freedom with a corresponding quantum number called color which can take three different values. Transition between different color states of quarks are generated by eight colored gluons and described by transformations belonging to the SU(3) group. Unlike the case of QED the gluons are charged, and can emit other gluons. The consequences of this fact leads to two important properties of the QCD, namely the confinement and the asymptotic freedom [16] of quarks.

It is found that the effective coupling constant goes to zero as the separation becomes very small. This behavior is known as asymptotic freedom. This is why the quarks nd gluons seem to be interacting weekly at short distances probed in hard collisions. Confinement means that quarks do not exist as isolated single particles but they exist only in bound systems which form a color singlet. The simplest two types of color neutral particles are mesons and baryons.

2.3 Neutrino-Nucleon Interaction

Neutrinos interact through exchange of a $W^{\pm}$ or a Z^0. When the interaction is through the $W^{\pm}$ the neutrino transforms into a charged lepton of the same generation, and this is referred to as a charged current (CC) event. When the interaction is through the Z^0 the neutrino preserves its nature; this is a neutral current (NC) interaction. In the case of neutral current interaction, it is impossible to reconstruct the kinematics of each event. In the following section, the kinematics of a charged current interaction will be presented.

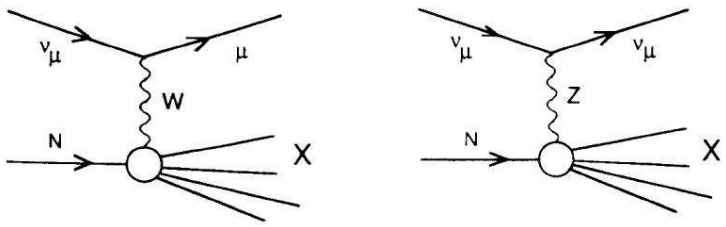

Figure 2.1: Feynmann diagrams of the ν_μ-nucleon, CC and NC interactions.

2.4 Charged Current Neutrino Interaction

Neutrino nucleon CC interaction is classified as deep-inelastic scattering (DIS), if the nucleon is broken up during the interaction, and as quasi-elastic scattering (QE) if the nucleon is left intact.

The charged current interaction of neutrinos off a nucleon is schematically shown in Figure 2.1. The final state consists of a muon and a hadronic shower:

$\nu(k) + N(p) \longrightarrow \mu(k') + X(p')$

where k, p, k' and p' are the four momenta. X corresponds to a set of n final state hadrons, each of which carries four-momentum p'_j. The four-momentum of the hadronic final state is

$$p' = \sum_{j=1}^{n} p'_j. \tag{2.5}$$

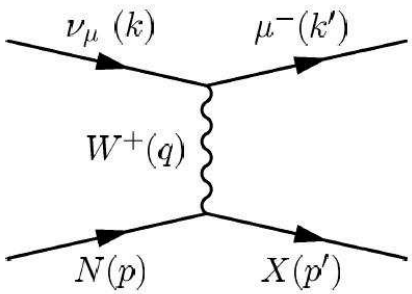

Figure 2.2: Feynmann diagram of the ν_μ CC interaction

The kinematics of this process is most conveniently described in terms of the following Lorentz-invariant quantities:

- $s = (k + p)^2$ Center-of-mass energy squared
- $Q^2 = -q^2$ Square of the 4-momentum transfer
- $\nu = \frac{p.q}{m} = E_\nu - E'_\mu$ Leptonic energy transfer
- $W^2 = (p')^2$ Invariant mass squared
- $x = \frac{Q^2}{2p.q}$ Bjorken x (scaling)
- $y = \frac{p.q}{p.k}$ Bjorken y (inelasticity)

where $q = k - k' = p' - p$ is the four-momentum transfer. We will choose the coordinate system in which the nucleon is at rest, the incoming neutrino travels along the X axis, and the outgoing muon makes an angle Θ_μ with respect to the neutrino direction. In this coordinate system, we find the following expression for the Lorentz-invariant quantities:

$$Q^2 = 2E_\nu(E_\mu - p_\mu \cos\Theta_\mu) - m_\mu^2 \approx 4E_\nu p_\mu \sin^2\frac{\Theta_\mu}{2}, \tag{2.6}$$

$$W^2 = M_N^2 - Q^2 + 2M_N E_{had}, \tag{2.7}$$

$$x = \frac{Q^2}{2M_N E_{had}}, \tag{2.8}$$

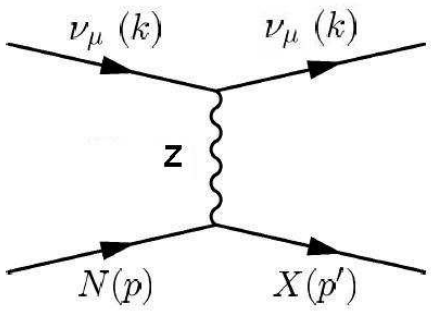

Figure 2.3: Feynmann diagram of the ν_μ NC interaction

2.5 Quasi-Elastic Scattering

The basic charged current neutrino-nucleon elastic interactions are:

$$\nu_l + n \rightarrow l^- + p, \tag{2.9}$$

$$\overline{\nu_l} + p \rightarrow l^+ + n. \tag{2.10}$$

where l can be τ or μ or e. Using the Feyman rules,

$$M = \frac{4G_F \cos\theta_c}{\sqrt{2}}[\overline{u}(\ell)\gamma^\mu \frac{1}{2}(1-\gamma_5)u(\nu_\ell)][\overline{u}(p)\gamma_\mu \frac{1}{2}\{F_v(q^2) + F_A(q^2)\gamma_5\}u(n)] \tag{2.11}$$

where F_v and F_A are form factors which appear since the proton and the neutron are not elementary particles. In the regime of small q^2, we use q^2=0. So the cross-sections involve the vector and axial vector weak charges of the neutron and proton $g_v = F_v(0)$ and $g_A = F_A(0)$ respectively.

2.6 The Parton Model

The parton model was introduced by R. P. Feynman [17] and J. D. Bjorken [18] to explain the new data on deep inelastic scattering of electrons on nucleons. The model views the nucleons as made up of point like constituents and provides a very simple framework for calculating scattering cross sections as well as structure functions for the nucleons. In the Parton Model, every object with finite size must have a form factor and therefore experience a dependence on the 4-momentum transfer from the scattered particle.

In the Parton Model, the struck nucleon act as a collection of a number of partons, such as: three valance quarks, sea quarks and antiquark pairs. The struck parton's final momentum obeys:

$$(xP + q)^2 = m^2 = 0, \tag{2.12}$$

$$x^2P^2 + 2xP.q + q^2 = 0. \tag{2.13}$$

Because $x^2P^2 << -q^2$, Eq.2.12. simplifies to:

$$x = \frac{-q^2}{2P.q} = \frac{Q^2}{2M\nu} \tag{2.14}$$

The relation between q^2 and $P.q$ was predicted by Bjorken. This hypothesis presents the idea that as $q^2 \to \infty$ and $\nu \to \infty$ the structure functions remain finite; so they must depend on the ratio of these two quantities. With this

observation the cross section is usually written as:

$$\frac{d^2\sigma^{\bar{\nu}\nu}}{dxdy} = \frac{G_F^2 ME}{\pi}((1-y)F_2^{\nu(\bar{\nu})}(x) + \frac{y^2}{2}2xF_1^{\nu(\bar{\nu})}(x) \pm y(1-\frac{y}{2})xF_3^{\nu(\bar{\nu})}(x)) \quad (2.15)$$

In the parton model, neutrinos are scattered by free quarks, anti-quarks and gluons. Neutrinos always have left-handed helicity, and they only interact with left-handed particles or right handed anti-particles. In the center of frame, the neutrino collides head on with the parton. The neutrino-quark system forms spin 0 state, and thus has a $(\frac{1+cos\theta}{2})$ cross section dependence. In the case of a neutrino interacting with a spin 0 particle one acquires an additional 2 $cos\frac{\theta}{2}$ term in the cross section. Since θ is related to y by the relation:

$$1 - y = \frac{1 + cos\theta}{2} \quad (2.16)$$

one finds:

$$\frac{d\sigma^{\nu q}}{dy} = \frac{d\sigma^{\bar{\nu} q}}{dy} = \frac{G_F^2}{\pi} \quad (2.17)$$

$$\frac{d\sigma^{\bar{q}\nu}}{dy} = \frac{d\sigma^{\bar{\nu} q}}{dy} = \frac{G_F^2}{\pi}(1-y)^2 \quad (2.18)$$

$$\frac{d\sigma^{\nu k}}{dy} = \frac{d\sigma^{\bar{\nu} k}}{dy} = \frac{G_F^2}{\pi}2(1-y) \quad (2.19)$$

One define $q(x, Q^2)$, $\bar{q}(x, Q^2)$, $k(x, Q^2)$ to be the probability of finding a particle of the appropriate type with fractional momentum x inside nucleon. This leads to the neutrino nucleon cross section:

$$\frac{d^2\sigma^{\bar{q}\nu}}{dxdy} = \frac{G^2xs}{\pi}(q(x) + \bar{q}(x)(1-y)^2 + k(x)2(1-y)) \tag{2.20}$$

$$\frac{d^2\sigma^{\bar{\nu}N}}{dxdy} = \frac{G^2xs}{\pi}(q(x)(1-y)^2 + \bar{q}(x) + k(x)2(1-y)) \tag{2.21}$$

Comparing with Equation 2.15, one can obtain:

$$2xF_1 = xq(x) + x\bar{q}(x), \tag{2.22}$$

$$F_2 = xq(x) + x\bar{q}(x) + 2k(x), \tag{2.23}$$

$$xF_3 = xq(x) - x\bar{q}(x). \tag{2.24}$$

2.6.1 Charm Production in Neutrino Charged Current Interaction

In the CC interaction neutrino interacts with "valence" d quark or "sea" s quark to produce c quark. Then by hadronization process, c quark "dresses" itself with other quarks or antiquarks from "valence" and "sea" quarks of the interacting nucleon so then a charm hadron is produced. Figure2.4 shows charmed hadron production by neutrino deep inelastic scattering.

Let us consider the seminclusive process

$$\nu_\mu N \to \mu^- cX$$

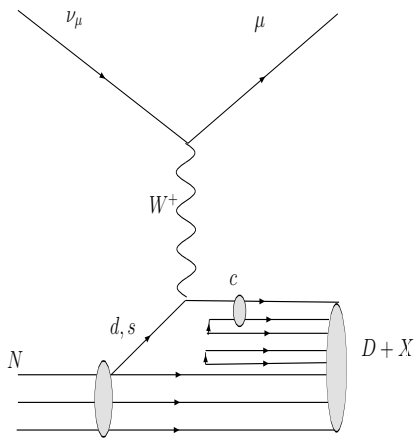

Figure 2.4: Charm production by ν_μ CC interaction

where X is a hadronic final state, and we neglect the hadronization of the final c quark.

We define:

$$2xF_1^c(x) = xF_3^c(x) = |V_{cd}|^2 xd(x) + |V_{cs}|^2 xs(x) \tag{2.25}$$

where V_{cd} and V_{cs} are CKM-matrix elements [13, 14].

At partonic level, the relevant processes for c production are [19]

$$\nu_\mu d \to \mu^- c \qquad \frac{d\sigma(\nu_\mu d \to \mu^- c)}{dy} = \frac{G_F^2 \hat{s}}{\pi}(1 - \frac{m_c^2}{\hat{s}})|V_{cd}|^2, \tag{2.26}$$

$$\nu_\mu s \to \mu^- c \qquad \frac{d\sigma(\nu_\mu s \to \mu^- c)}{dy} = \frac{G_F^2 \hat{s}}{\pi}(1 - \frac{m_c^2}{\hat{s}})|V_{cs}|^2. \tag{2.27}$$

The production of c quark through $\nu_\mu d$ scattering is Cabibbo suppressed ($|V_{cd}|^2 \sim \sin^2\theta_c \simeq 0.04$), while the production through $\nu_\mu s$ scattering ($|V_{cs}|^2 \sim \cos^2\theta_c \simeq 0.96$) is instead suppressed by the low abundance of s quarks in the sea.

If $\hat{p} = \xi p$ is the parton four-momentum, if a c quark is produced in the final state, and neglecting the initial parton mass ($m_d, m_s \ll m_c$), we have

$$m_c^2 = (\hat{p} + q)^2 = -Q^2 + 2\xi p.q = -Q^2 + \frac{\xi Q^2}{x}. \tag{2.28}$$

The parton distribution will be probed at

$$\xi = x(1 + \frac{m_c^2}{Q^2}) \tag{2.29}$$

which is called the *slow rescaling* variable [27, 28].

The cross section for charm production induced by neutrino scattering off an isoscalar target T then reads

$$\frac{d\sigma(\nu_\mu T \to \mu^- cX)}{dxdy} = \frac{G_F^2 s\xi}{2\pi}[(u(\xi) + d(\xi))|V_{cd}|^2 + 2s(\xi)|V_{cs}|^2](1 - \frac{m_c^2}{s\xi})\theta(\xi - \frac{m_c^2}{s}). \tag{2.30}$$

Since $\hat{s} = (\xi p + k)^2 \simeq \xi s$, we can replace the kinematic factor $(1 - \frac{m_c^2}{s\xi})$ in Eq.(2.30), with $(1 - \frac{m_c^2}{\hat{s}})$, and with the further assumption $s(x) = \overline{s}(x) = c(x) = \overline{c}(x)$, we get

$$\frac{\sigma(\nu_\mu T \to \mu^- cX)}{\sigma(\nu_\mu T \to \mu^- X)} \simeq \frac{(U + D)|V_{cd}|^2 + 2S|V_{cs}|^2}{U + D + 2S + \frac{1}{3}(\overline{U} + \overline{D} + 2\overline{S})}(1 - \frac{m_c^2}{\hat{s}}) \tag{2.31}$$

where

$$Q = \int_0^1 xq(x)dx, \qquad Q = U, D, S \tag{2.32}$$

is the fraction of nucleon's momentum carried by q quarks.

CHAPTER 3

THE CHORUS DETECTOR

The major aim of the CHORUS (CERN Hybrid Oscillation Research ApparatUS) experiment is to search for $\nu_\mu \rightarrow \nu_\tau$ oscillations in the wideband neutrino beam of the CERN SPS, but the improvement of the automatic scanning system in the experiment allows also efficient search for charmed hadrons with a high statistics.

The CHORUS detector [29] consists of the emulsion target, a scintillating fiber tracker system, hadron spectrometer, electromagnetic and hadronic calorimeters , a muon spectrometer, and a trigger system. In the following sections detailed description of all the systems of the detector can be found. CHORUS detector layout can be seen in Figure 3.1.

3.1 The Neutrino Beam

The neutrino beam for this experiment was the West Area Neutrino Facility (WANF) [30] of the CERN SPS. The protons are accelerated to an energy of 450 GeV in the CERN SPS and directed onto a beryllium target. The beryllium target was composed of 11 rods of 10 cm length and 3 mm diameter spaced 9

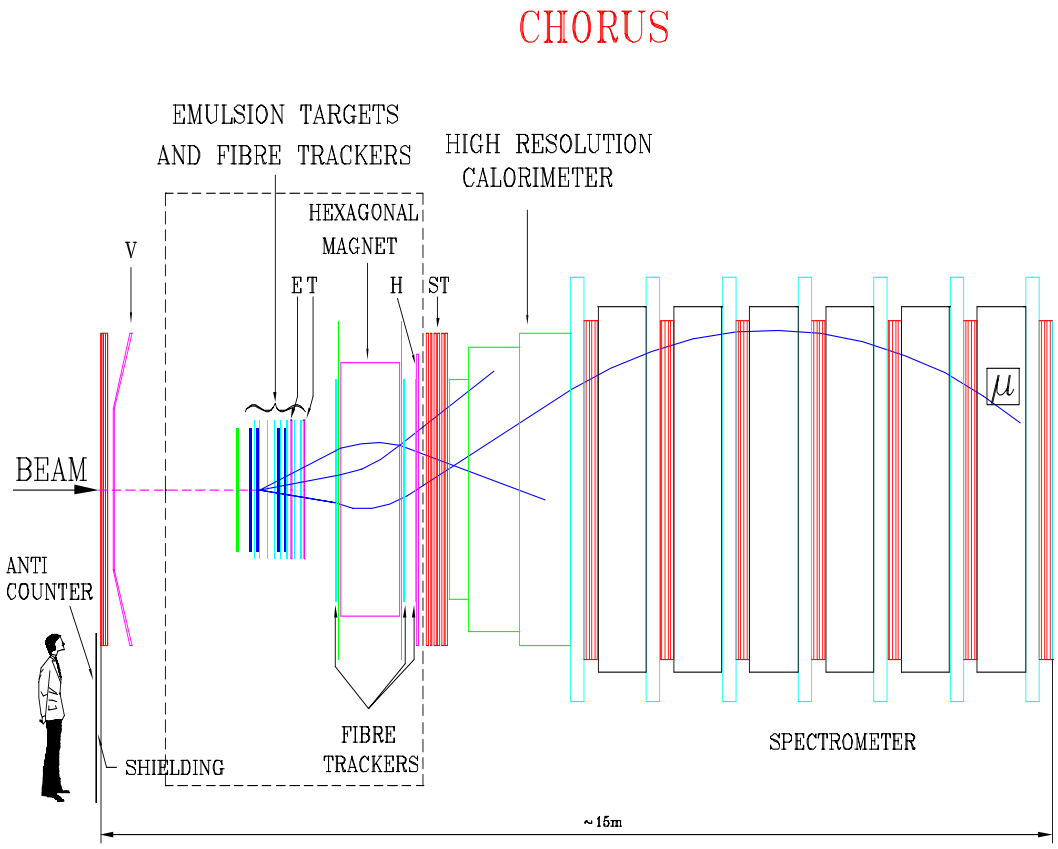

Figure 3.1: CHORUS detector layout.

cm apart from each other to minimize the interactions of produced pions and kaons. Then positive mesons are focused (negatives are defocused) by 2 air core magnets called the horn and the reflector. Focusing and defocusing mesons help to minimize anti-neutrino contamination. After the two magnetic lenses, in a 290 m long vacuum tunnel, these pion and kaon mesons decay to ν_μ dominantly. A schematic view of the beam line is seen in Figure 3.2. The energy spectra of the components is shown in Figure 3.3 and the relative abundance of the different neutrino flavors in the beam is given in Table 3.1. The neutrino beam has an

upward slope of 42 mrad. The detector parts were centered along this slope, however, every part is placed vertically.

Table 3.1: The relative abundance of the different neutrino flavors in the beam

Neutrino type	Relative Abundance (%)	<E> (Gev)
Muon neutrino	100	26.9
Muon anti-neutrino	5.6	21.7
Electron neutrino	0.7	47.9
Electron anti-neutrino	0.17	35.3

3.2 Emulsion Target

The emulsion target is the first part of the emulsion set-up; it records the neutrino interactions. The second part is composed of thin emulsion sheets; they are used as a high-accuracy interface between fiber trackers and target. The emulsion target is 260 l in volume, and 770 kg in mass. It consists of 4 emulsion stacks, each of which has dimensions of 1.42x1.44 m^2 and has 8 modules. Modules are made up of 36 individual emulsion sheets (or plates) which have two layers of emulsion gel on either side of a plastic base. The thickness of the base is 90 μm and the depth of each of the emulsion layers is 350 μm. A 800 μm thick plastic base and two gel layers of 100 μm depth compose the interface sheets. The different gel and base thicknesses help maximize the angular resolution to match the electronic detector event with the emulsion event. The emulsion set-up was kept at a temperature of $5C$ to reduce fading.

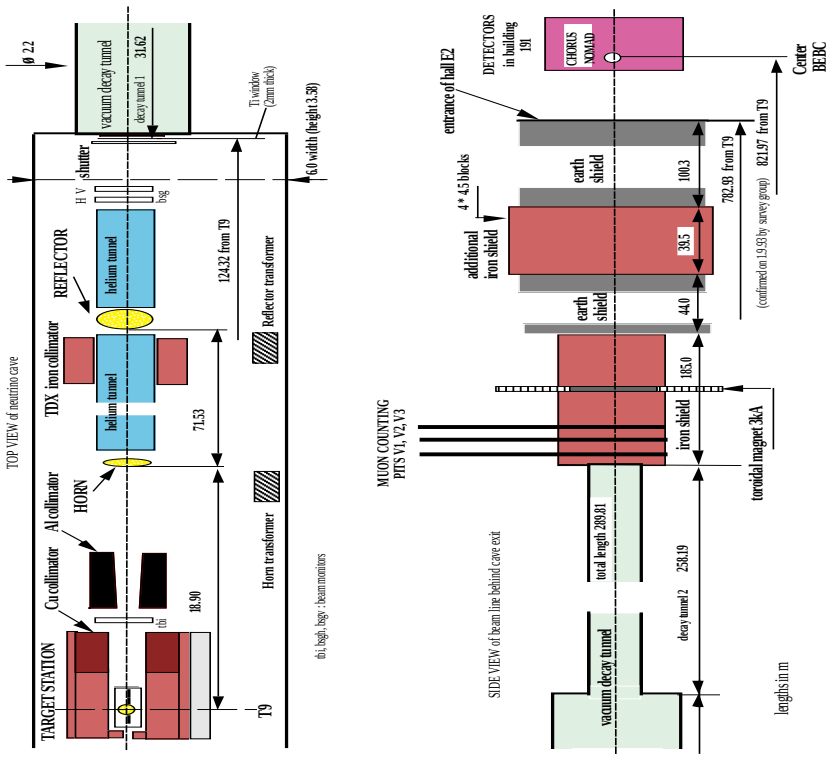

Figure 3.2: A schematic view of the beam line.

3.3 The Scintillating Fiber Tracker

The tracker system consists of two components: the target tracker and the diamond-shaped magnet tracker. It was built assembling more than 1 million plastic scintillating fibers of 500 μm in diameter. The basic element of this tracker is one scintillating fiber. A fiber has a polystyrene core that emits photons when traversed by a particle. A 3.2 mm thick cladding material surrounds the core with smaller refraction index than the core, thus realizing a light guide. The fibers are bundled together in to ribbons of 7 staggered planes. A tracker plane consists

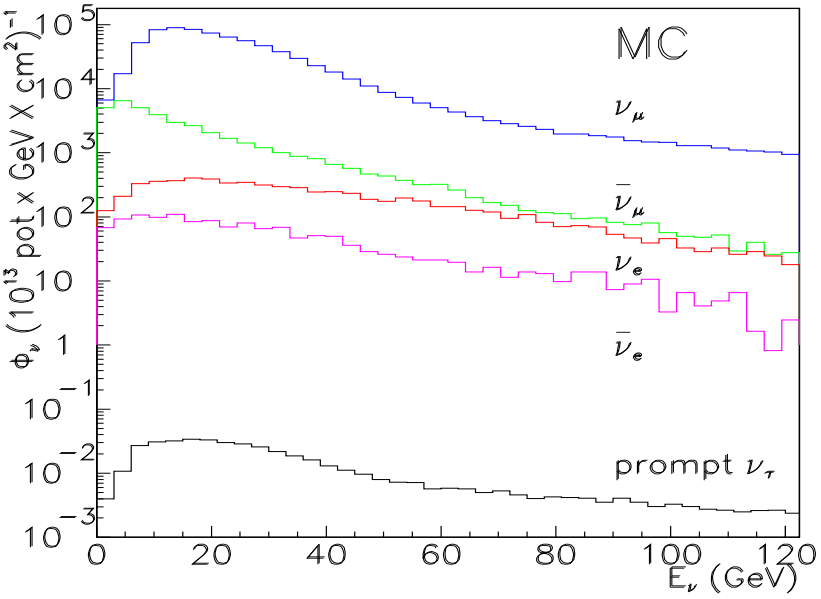

Figure 3.3: Neutrino beam composition

of four ribbons with different orientations (X, Z, $X^{\pm}$, $Z^{\pm}$ rotated by ± 8 degree relative to Y and Z, thus making the resolution of ambiguities easy). The target tracker (TT) locates the stack where the neutrino interaction takes place, and makes accurate predictions at the interface emulsion sheets. There are 8 target tracker modules altogether, interleaved between the 4 target emulsion stacks. The using information from these 4 projections, three-dimensional trajectories of traversing particles can be reconstructed. The magnet tracker measures the charge and momentum of the particles originating from a neutrino interaction

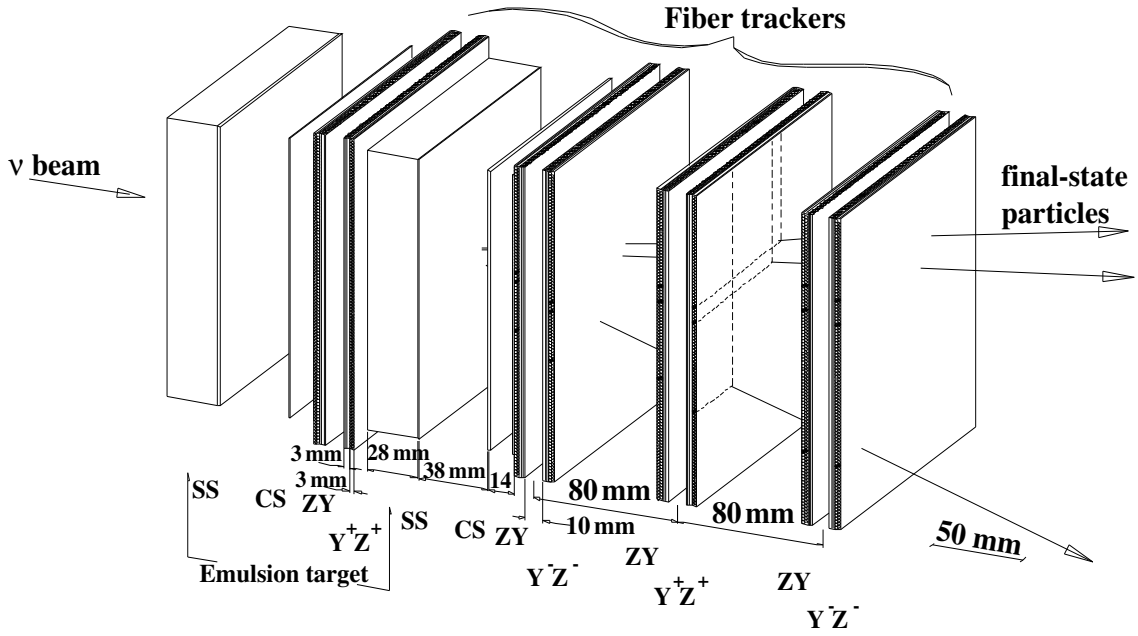

Figure 3.4: Schematic view of the CHORUS target

at the target. At the read-out ends, there are 58 optoelectronic chains, each consisting of four image intensifiers and CCD camera. A maximum number of two events for spill could be recorded.

3.4 Hadron Spectrometer

Hadron spectrometer was located between the target region and the calorimeter. It measures the charge and momentum of particles before they enter the calorimeter. It is also used to determine the momentum of the muons that don't

reach the muon spectrometer.

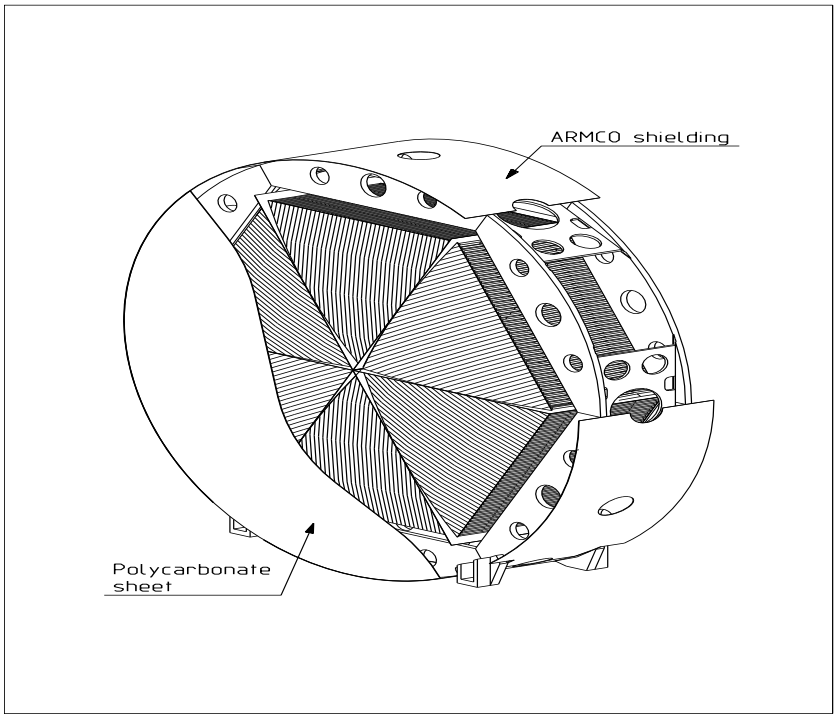

Figure 3.5: Hexagonal Magnet

The hadron spectrometer consists of an air-core magnet of hexagonal shape (Figure 3.5) with a torodial field and 3 fiber tracker planes. The magnet was made of six equilateral triangles with 1.5 m sides and 0.75 m depth. It produces a homogeneous field of 0.12 Tesla parallel to the outer side.

The three fiber trackers measure the particle position and slope before and after the magnetic field. The momentum resolution $\Delta P/P$ of the magnet tracker results from the quadratic combination of two terms: a constant term, evaluated

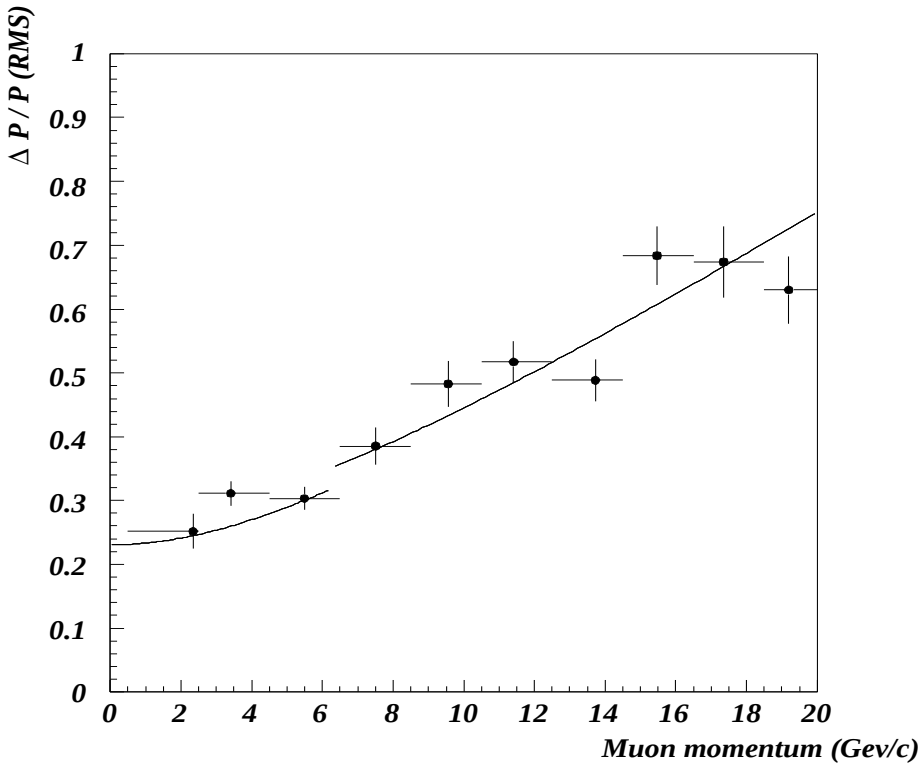

Figure 3.6: Momentum Resolution for a Single Track event

at 22 %, from the multiple scattering and the term proportional to particle momentum, which reflects the measurement accuracy. The design performance of the DT should have given a relative error on the momentum measurement of the form.

The tracker resolution is given by:

$$\Delta P/P = [(0.22)^2 + (0.035p)^2]^{1/2} \tag{3.1}$$

Because of residual alignment, the streamer tubes have been replaced with

honeycomb chambers (August 1996) and three Emulsion Tracker have been installed, to overcome bad tracker resolution.

3.5 The Calorimeter

The calorimeter [31] shown in Figure 3.7 is used to measure the energy of the particles and confirm the momentum measured in hadronic spectrometer. Muons are tracked in this part before they arrive at the muon spectrometer. The calorimeter consists of three parts with decreasing granularity called, electromagnetic sector (EM) the first hadronic sector (HAD1) and the second hadronic sector (HAD2). The EM part contains four planes with 31 modules, and in each module there are 740 fibers. These fibers are assembled into two bundles on both sides of a module. Each bundle is coupled to a Photo-multiplier tube (PMT) via a Plexiglas light guide. The HAD1 part is composed of 5 planes and each plane contains 40 modules. There are 43 layers of lead and 1554 scintillating plastic fibers in each module. The fibers are collected into one bundle and coupled via a light guide to a PMT at both ends. The HAD2 part contains 18 modules, each of which is built as a sandwich of five layers of lead with a thickness of 1.6 cm and five layers of 4 mm thick scintillator strips, packed in 1 mm steel. The modules are 369 cm long and 20 cm wide. Each module is coupled to four PMT's via light guides, two on either side.

For different momenta in the range from 2.5 to 10 GeV/c, the electron response

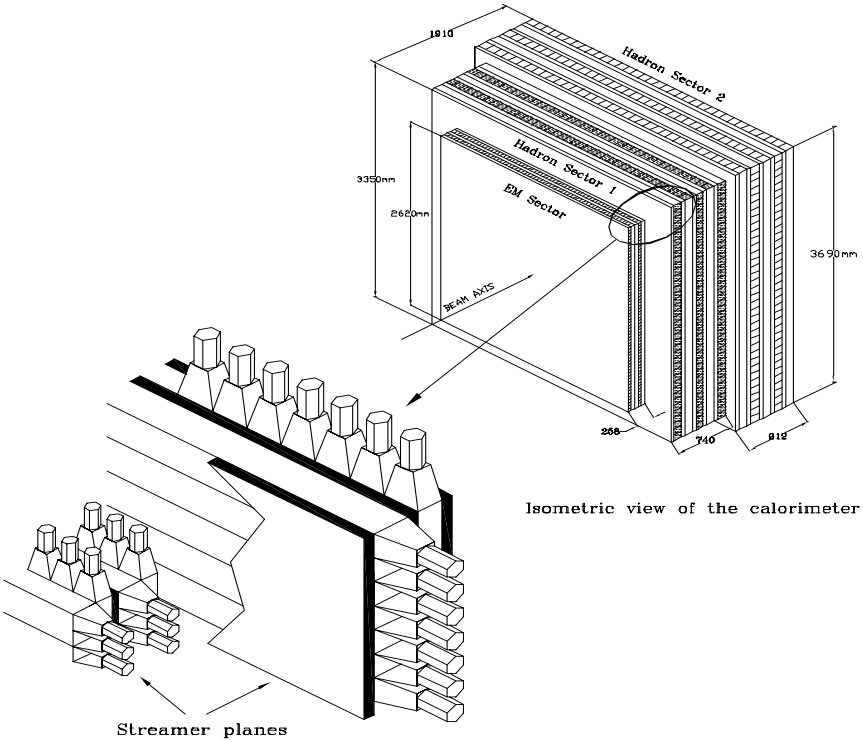

Figure 3.7: Isometric view of the calorimeter

was studied. For each momentum, a Gaussian fit is performed to the distribution of the calorimeter signal. The energy dependence for electrons is well fitted by the function:

$$\frac{\sigma(E)}{E} = \frac{(13.8 \pm 0.9)\%}{\sqrt{E(GeV)}} + (-0.2 \pm 0.4)\% \tag{3.2}$$

The result agrees with the Monte Carlo predictions. The response to pions was studied in the range from 3 to 20 GeV/c. The energy resolution can be determined from a Gaussian fit to the response distributions. The energy dependence of the

hadronic resolution is parametrized as:

$$\frac{\sigma(E)}{E} = \frac{(33.3 \pm 2.4)\%}{\sqrt{E(GeV)}} + (1.4 \pm 0.7)\%. \tag{3.3}$$

The predictions of a Monte Carlo simulation are consistent with the data.

3.6 Muon Spectrometer

The muon spectrometer is used to identify muons and determine their charge, trajectory and momentum. The schematic view of the spectrometer is shown in Figure 3.8. The spectrometer located after the calorimeter. Only the muons having energy greater than 1.5 GeV can reach this part since the calorimeter absorbs the rest.

The spectrometer consists of six magnetized iron toroid modules and tracking detectors made of drift chambers and streamer tubes. In addition, scintillating interleaved with the magnet iron provide a measure of the leak from the calorimeter. The scintillating counters provide fast trigger signals. The momentum resolution of the muon spectrometer is about 19% percent at 70 GeV. For lower momenta, a Monte Carlo simulation is used to determine the muon momentum resolution.

3.7 The Trigger System

The trigger, shown in Figure 3.10, is used to select neutrino interactions in the target and to reject background events from cosmic rays, beam muons and

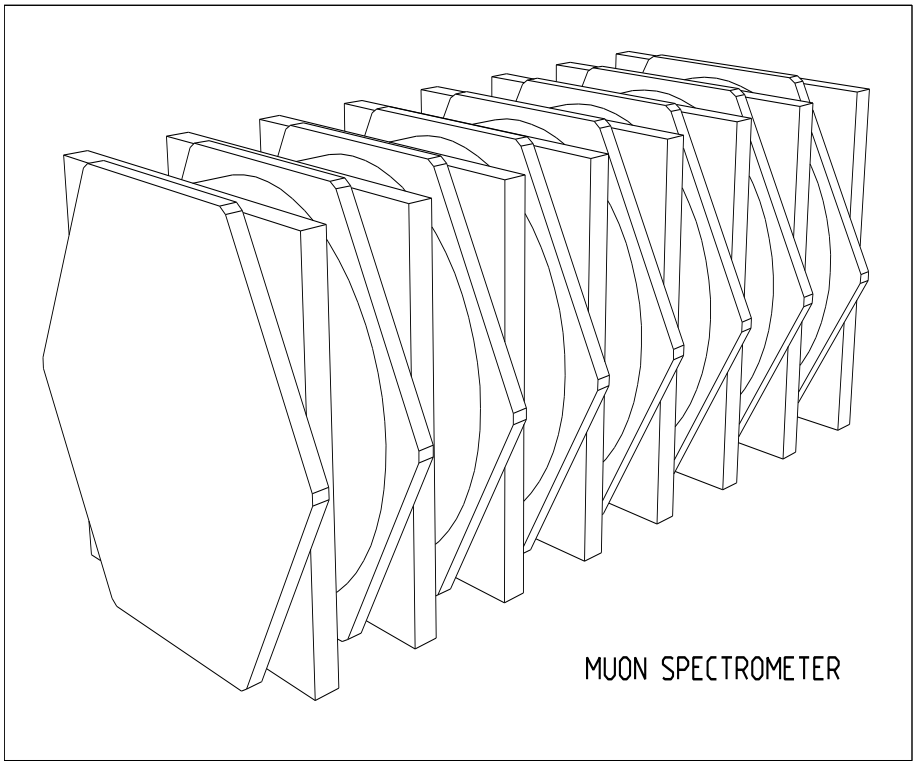

Figure 3.8: Muon Spectrometer

neutrino interactions outside the target. The trigger consists of scintillator planes named E, T, H, V and A. A neutrino trigger in the target region is defined by a coincidence hit in E, T and H consistent with a particle trajectory with $\Theta < 0.25$ rad with respect to the neutrino beam direction. A veto is formed by any combination of a counter hit in the veto hodoscopes (V and A), and a hit in T, with precise timing to avoid vetoes due backscattering of particles coming from neutrino interactions in the target. The measured rate of neutrino interactions is 0.5 events per 1013 proton on Be target corresponding to an effective target mass

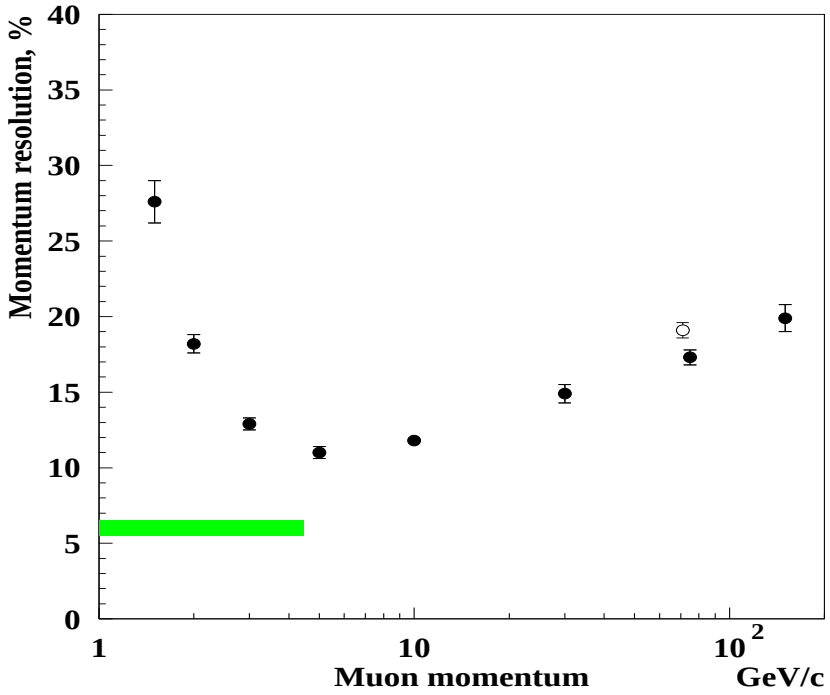

Figure 3.9: Momentum Resolution

of 1600 kg. The fraction of events originated from emulsions is 50%. The trigger efficiency is about 90% for ν_μ neutral current interactions and raises to 99% for charged current events.

3.8 The Emulsion Scanning

The information of the electronic detectors has been used to define two data sets, 0μ and 1μ samples (shown in Figure 3.11 and 3.12) distinguished by the

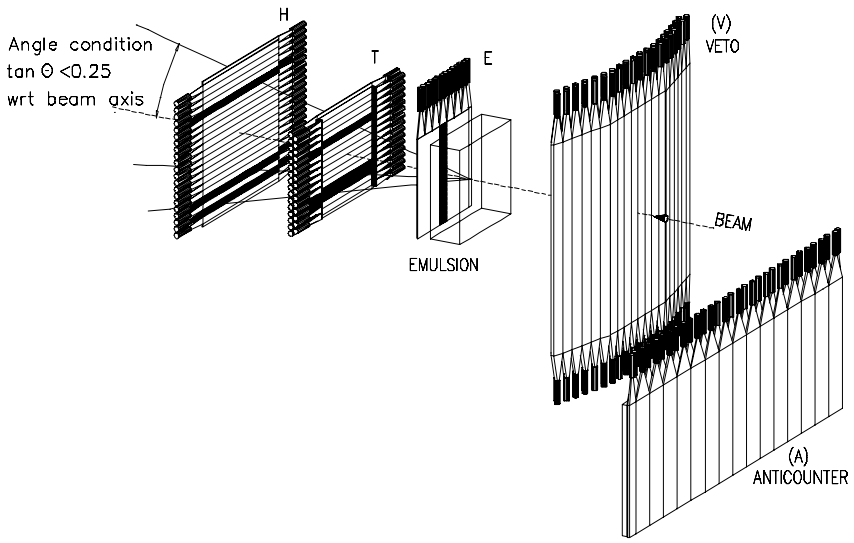

Figure 3.10: Schematic view of the trigger system

presence or absence of one reconstructed muon of negative charge. For each sample few kinematical selections are applied to reduce the scanning load, while keeping a high sensitivity . The resulting $1\mu(0\mu)$ sample consists of 477.600(335.398) events with a reconstructed vertex in emulsion. The reconstructed tracks in the fiber tracker are used to guide scanning in the emulsion.

The emulsion scanning of the event starts from the extrapolation of the tracks reconstructed in The Fibre Tracker to the most downstream interface emulsion sheet called changeable sheet (CS). All selected tracks ('scan-back tracks') are

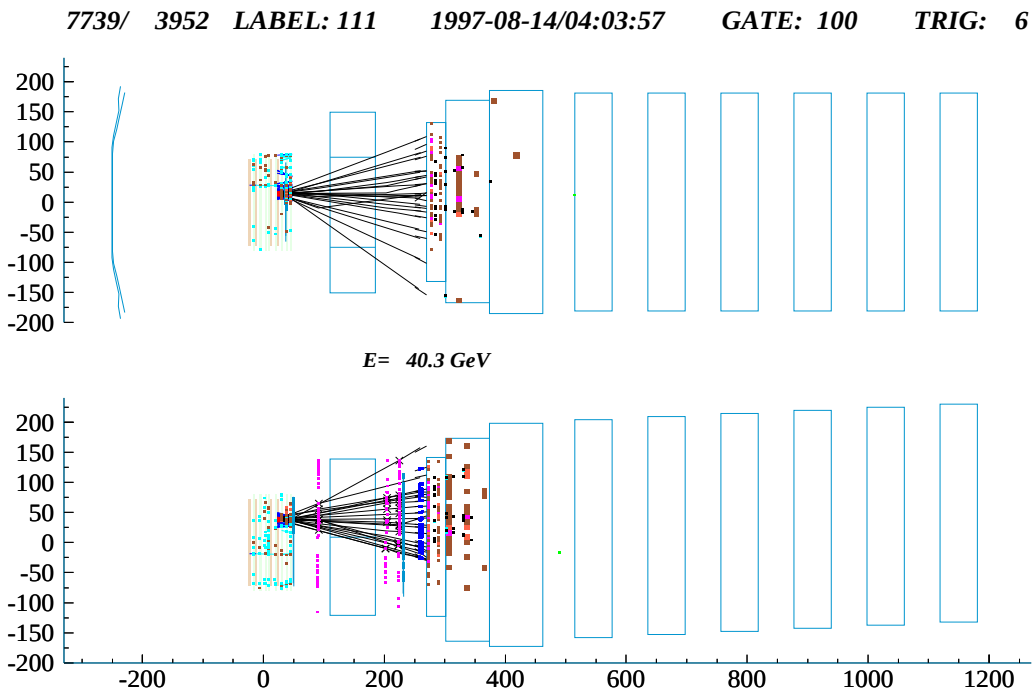

Figure 3.11: CHORUS 0μ event.

searched for in the emulsion interface sheets. The track segments found in these sheets are then used to predict with high precision the position and the angle of the track in the emulsion stack. If found, this track is then followed upstream from plate to plate. In each plate, only the most upstream 100 μm layer is scanned searching for a track with the similar slope as the one measured in the emulsion interface sheets. The interaction vertex is assumed to be located if the track is not observed in two consecutive plates, the first of which is defined as the vertex plate.

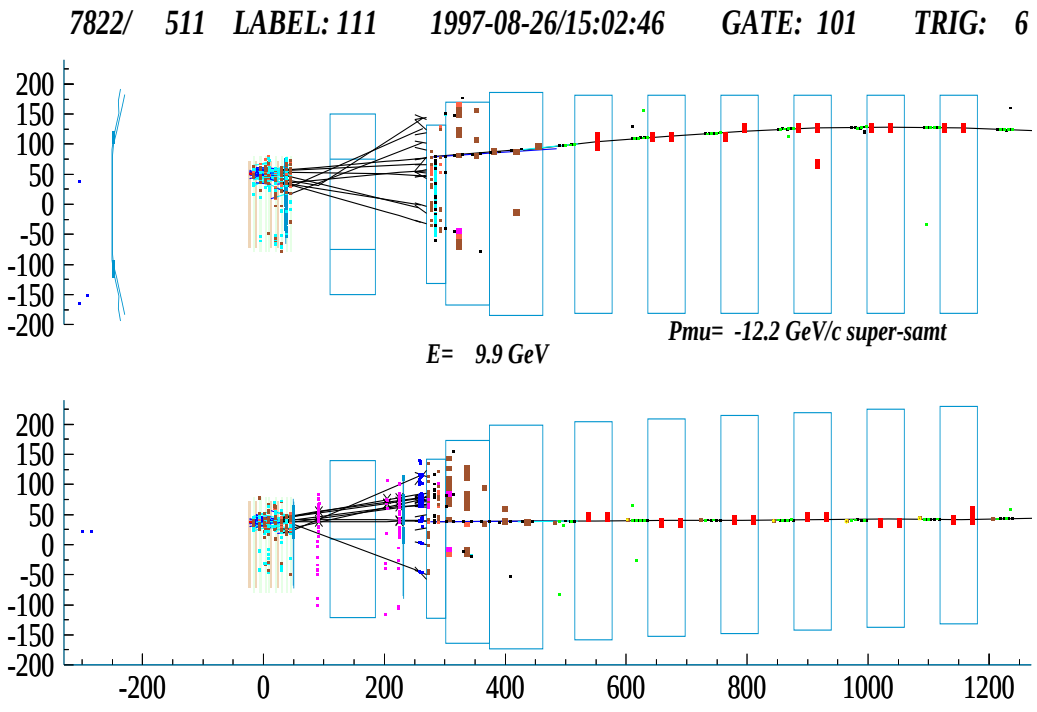

Figure 3.12: CHORUS 1μ event.

3.8.1 Changeable Sheet (CS) Scanning

For selected events, SB parameters: slopes and positions, reconstructed in the fiber tracker, are used to guide the scan in the most downstream interface emulsion sheet. An automatic scanning is performed within 11x11 (1080x810 μm^2) views around extrapolated position of Scan Back (SB) track. A track is taken as a candidate if the angle difference, $\Delta\Theta$, between predicted (fiber reconstructed) and measured angles is less than 30 mrad. Scanning is finished for that prediction, all the found candidates undergo checks for further selection to

keep the good candidates for Special Sheets (SS) scanning that is in next plate (upstream) to CS.

3.8.2 Special Sheet (SS) Scanning

After finding the track in CS they are followed in Special Sheet (SS), using position and slope information from CS scanning. SS scanning is performed within the 7x7 microscope views (800 x 700 μm^2) centered about predicted position

3.8.3 Vertex Location

SB track found in the SS is then followed in the upstream direction plate by plate in the bulk emulsion using track segments in the most upstream, $100\mu m$ of each plate. The measurement position in the bulk plate n+1. Track is said to be found in the bulk plate.

If the SB track is not found in two successive emulsion plates (lets say **n** and **n+1**), plate n, is decided to be a vertex plate which is supposed to contain the neutrino interaction or the decay vertex (or both) shown in Figure 3.11. A detailed description of event location can be found in [32].

3.9 Netscan

Netscan is a new method for event location and decay search in emulsion developed in Nagoya University for the DONUT experiment [12]. The procedure

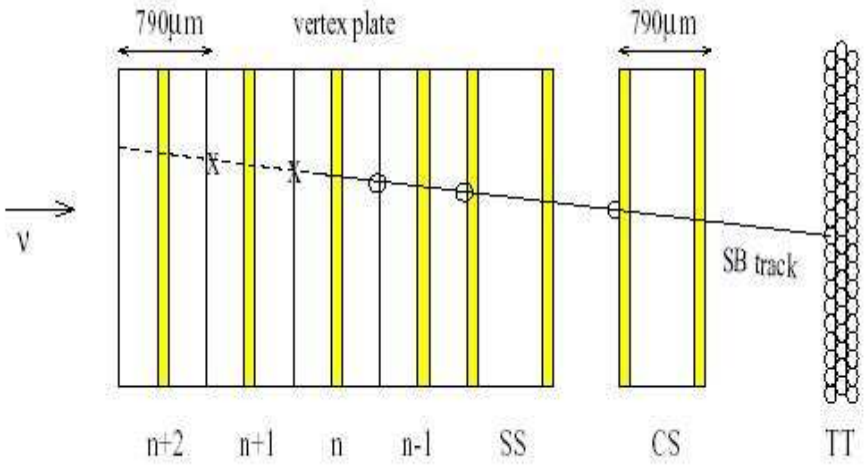

Figure 3.13: Event Location

is described in detail in reference [34].

Main principle of this method is to pick up all tracks in the fiducial volume corresponding to every prediction. In order to identify particle's decay, a volume of $1.5 \times 1.5 \times 6.32mm^3$ around. The located vertex position was scanned with a very fast scanning system UTS.

The parameters (positions, slopes, pulse, height etc.) of all track segments with angle below 400mrad found in the fiducial volume are stored in the database. Typically, 5000 track segments are recorded per event with the scanning systems used, the Netscan of one event takes about 11 minutes.

In the Phase I, following the SB track as a until the vertex plate "called scan back location", also used in Phase II as a located events for prediction for Net

Scanning.

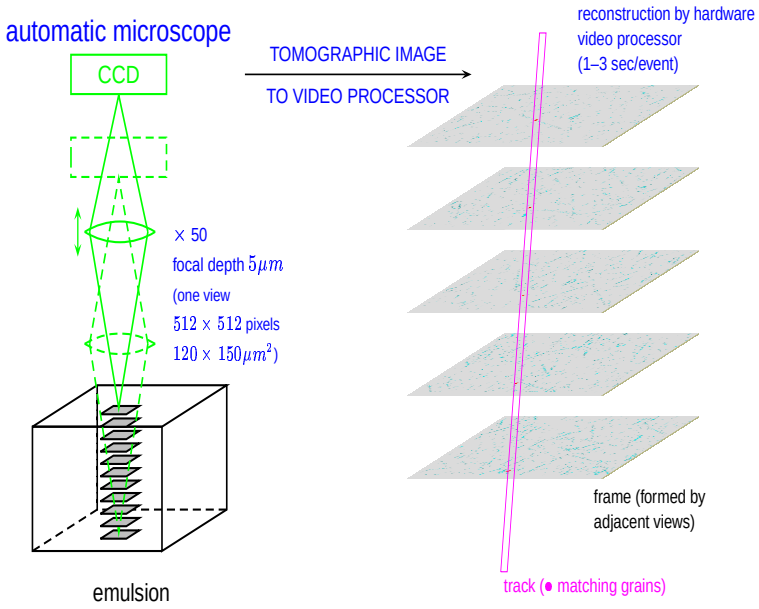

Figure 3.14: Schematic description of the track reconstruction procedure in the automatic scanning system.

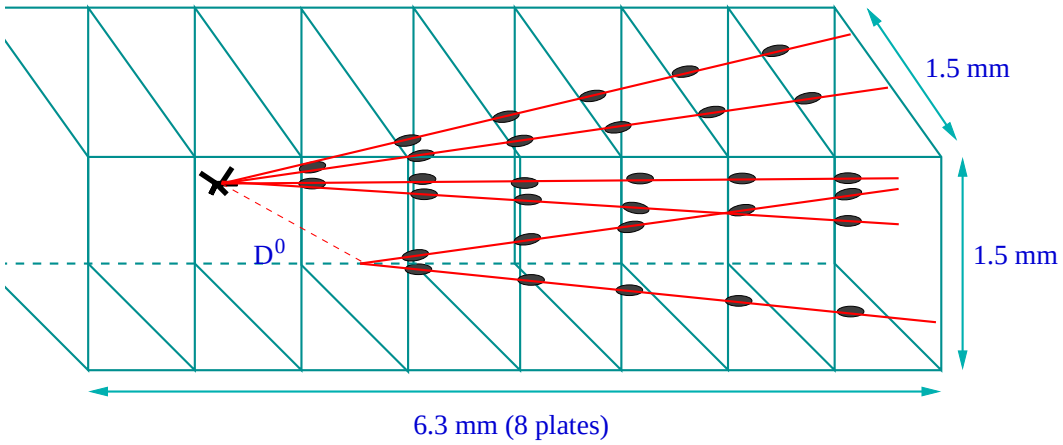

Figure 3.15: Schematic view of the Net Scanning fiducial volume.

Table 3.2: The composition of the CHORUS emulsion

Element	Atomic number	Weight (%)	Mole fraction (%)
Iodine	53	0.3	0.06
Silver	47	45.5	11.2
Bromine	36	33.4	11.1
Sulfur	16	0.2	0.2
Oxygen	8	6.8	11.3
Nitrogen	7	3.1	5.9
Carbon	6	9.3	20.6
Hydrogen	1	1.5	40.0

CHAPTER 4

EVENT RECONSTRUCTION AND SIMULATION

This chapter gives a brief overview of Monte Carlo programs used in CHORUS. Monte Carlo (MC) is an essential part of the CHORUS experiment. It includes the modeling the neutrino beam, the generation of neutrino events, simulation of the detector response and the reconstruction.

4.1 Introduction to Monte Carlo Methods

Numerical methods that are known as Monte Carlo methods can be loosely described as statistical simulation methods, where statistical simulation is defined in quite general terms to be any method that utilizes sequences of random numbers to perform the simulation. Monte Carlo is now used routinely in many diverse fields, from the simulation of complex physical phenomena such as radiation transport in the earth's atmosphere to the simulation of the esoteric sub-nuclear processes in high-energy physics experiments.The only requirement is that the physical (or mathematical) system be described by probability density functions (pdf's). Once the pdf's are known, the Monte Carlo simulation can proceed by

random sampling from the pdf's.

Briefly, the term Monte-Carlo refers to a group of methods in which physical or mathematical problems are simulated by using random numbers.

4.2 MC Simulation of Neutrino Interactions in the CHORUS Detector

The first step of the MC simulation of events in the CHORUS detector is the simulation of the neutrino beam. The neutrino beam generator, which is called GBEAM [35] describes the interaction of SPS beam protons with the WANF beryllium target for the production of mesons. The parent mesons are modeled with FLUKA [36] tracked subsequently through the horn, reflector and the decay tunnel. Their decay produces neutrinos with given flavor, creation-vertex and four-momentum. The incoming neutrino information produced by GBEAM is used as input to all event generators in CHORUS.

The current version of GBEAM includes the present best geometrical description of the beam line. The geometrical description has been modified including all the new features of the beam line and the different CHORUS detector position.The tools have been introduced to study in detail the hadronic shower evolution along all the beam line, from the beryllium target to the decay tunnel.

4.3 Event Generators in CHORUS

The event generator will select the initial and final state of the neutrino interaction. The initial state is defined by the incident neutrino, which is simulated by GBEAM and described by its four-vector and lepton type (muon), and the struck nucleus, which is chosen by considering the relative abundance of different nuclei types in the detector, plus the nucleon which is assigned some Fermi momentum. The products of the neutrino interaction depend upon the cross-section of the available neutrino scattering process at the neutrino incident energy and are described by the particle types and four-vector momentum. The neutrino interaction cross-sections are based on theoretical models, which are fitted to data from neutrino scattering experiments on various targets. For the energy range relevant to atmospheric neutrinos, cross-sections have been measured in bubble chamber experiments. At low energies, charged current neutrino-hadron interactions are predominantly quasi-elastic and single pion production, in which the neutrino scatters off an entire nucleon rather than the constituent partons. Neutrino charged current interactions can also produce baryon resonances, which decay to final states consisting of a proton or neutron and at least one pion. Deep inelastic interactions in which the neutrino scatters off individual partons in the nucleus contribute little to the atmospheric neutrino interaction cross-sections, since they come into effect above 5 GeV. Nuclear Fermi momentum and its effect

on the final state momentum of the event is taken into account in the simulation. The nucleus is described as a degenerate fermion gas with filled energy states up to the Fermi momentum. A final state nucleon produced with momentum less than the Fermi momentum for the material is forbidden by the Pauli exclusion principle. Pauli blocking is taken into account in CHORUS for elastic and quasi-elastic events. Finally, the final state nucleus may be produced in an excited state, from which it will decay by emitting low energy particles. Such nuclear decays are not simulated in CHORUS .

4.3.1 JETTA

Simulation of deep inelastic ν_μ charged current interactions comes from JETTA [39, 40](JETS in TAU Analysis), the standard CHORUS event generator. It is based on the LEPTO [37] package to simulate ν_μ charged current interactions, and JETSET for quark hadronization and decays of short lived particles, with some peculiar modifications for CHORUS, and can describe neutrino interactions with $q^2 > 2\ GeV^2/c^2$.

In JETTA, the nucleon structure functions are parameterized according to GRV94LO [38], and the nuclei have a Fermi motion parameterized by $dn/dE_{kin} \alpha \sqrt{E_{kin}}$, with a maximum kinetic energy of 27 MeV.

The charm quark hadronization is parameterized according to the Peterson fragmentation function, and the charmed hadrons produced are D^0, D^+, $D_{\pm s}$, Λ_c,

the same fragmentation being used for all of them. The transverse momentum distribution was parameterized as $dn/dp\ \alpha\ e^{\beta p^2}$. The starting values of the relative fractions of charmed hadrons in the c quark hadronization are taken from reanalysis of the E531 data.

JETTA reproduces reasonably well neutrino bubble chamber experimental data on charged track multiplicities, transverse shower development, pion energies and fragmentation functions for hadrons.

4.3.2 RESQUE

RESQUE [41], is an event generator of Quasi-Elastic neutrino interactions. The computation of total and differential cross-sections and resonance decays have been adapted from the Soudan-II RSQ generator. The main changes concern extension of the energy range for the calculation of cross-section and for the generation of events (by one order of magnitude) which is done according to the CHORUS beam spectrum. The nuclear effects, Fermi motion and the Pauli suppression are considered together with the incorporation of ν_τ interactions, and tau decays taking into account the polarization of the lepton in the final state.

Three nucleon form factors are used in the calculation of QE and CC cross sections. The fourth form factor which is proportional to mass squared of the outgoing lepton, is taken in the case of ν_τ interactions.

The original routines from RSQ code are used to generate the contribution

of 16 baryonic resonances (N and Delta) with invariant-mass less than 2 GeV. All resonances and their decays are generated separately. The production cross-sections have been computed by Rein and Seghal using the FKR semirelativistic quark model.

4.4 The Detector Simulation

The simulation of the passage of elementary particles through the matter is performed with GEANT which was developed at CERN. It is based on MC techniques for the generation of pseudo data, which can be processed and analyzed like the real data of the experiment.

The main principal of GEANT is; transporting of particles through the detector for the simulation of detector response with graphical representation of the setup and of the particle trajectories.

The program allows the user some properties, such as; describing an experimental setup by a structure of geometrical volumes., accepting events simulated by MC generators, transporting particles through the various regions of the setup with taking into account geometrical volume boundaries and physical effects according to the nature of the particles themselves, their interactions with matter and the magnetic field, recording particle trajectories and the response of the sensitive detectors, visualizing the detectors and the particle trajectories.

GEANT is originally designed for the High Energy Physics experiments but

today it has applications in medical and biological sciences, radio-protection and astronautics.

In the CHORUS detector the simulation of the interactions and shower development is done by EFICASS (Emulsion FIbers. CAlorimeter and Spectrometer Simulation) it contains a very detailed description of the detector in the GEANT framework.

EFICASS contains the geometrical setup of the detector, takes care of the tracking of the particles through active and passive media, and converts the information of the active elements into detector 'signal', representing the calibrated raw data response of the apparatus. These signal are stored in the same format as delivered by the DAQ system in order to be processed in the same way as the real data by the same reconstruction and analysis programme CHANT. The detailed simulation of the detector response is the main aim of EFICASS.

The longitudinal vertex positioning is performed with a special algorithm in accordance with material density the neutrino traverses. EFICASS digitizes GEANT hits in each active volume of the CHORUS detector. Its output, similar to what is produced by data acquisition system, is sent to the reconstruction program

4.5 Event Reconstruction and Analysis

CHANT (CHorus ANalysis Tool) is a basic CHORUS off-line data processing program. It's aim is to provide a unified access to the CHORUS experimental and MC data.

The event reconstruction starts with the pattern recognition in the electronic detectors. Tracks are found in the fiber-tracker in the target region and, independently, in the muon spectrometer. A matching is attempted between these two sets of tracks in order to identify primary muons. Vertices are defined using the points of closest approach of the fibre-tracker tracks. The primary vertex is the most upstream one that contains a muon.

The selection of candidate tracks to be used for the event reconstruction was based on a χ^2 matching probability in the angular and position variables. For all the events with a primary vertex reconstructed inside the emulsion stacks, track information is used to search for the interaction point in the emulsion target.

4.6 Comparison of Data and Monte Carlo

The data set used for the comparison is from 1996 and 1997 data taking. In total 100270 events have been located and Netscanned with the procedure described in Chapter 3. The breakdown of the data sample is given in Table 4.1.

We have compared the following quantities:

- Number of reconstructed tracks at the primary vertex.
- Muon Momentum.
- Total energy deposited in the calorimeter.
- Muon slopes, θ_y and θ_z.
- Q^2, square of four momentum transfer.
- Bjorken-x.
- Bjorken-y.
- W^2, square of invariant mass.

A large sample of deep-inelastic neutrino interactions (DIS) were generated according to the beam spectrum of the CHORUS ν_μ. Quasi-elastic (QE) interactions and resonance production events are modeled with the RESQUE package code with a rate of 9.6 % relative to DIS in the neutrino case and of 26 % in the antineutrino case. The generated events are passed through GEANT

Table 4.1: The data flow for both 1996-1997 data and MC.

	1996	1997	MC
Located in emulsion	42639	57531	36411
$E_{cal.} > 0$	37611	50497	32343
$E_{sh.} > 0$	34905	47476	32296
$P_{\mu^-} < 0$	28223	38571	32296

based simulation of the CHORUS detector and through the same reconstruction program, CHANT, as used for the experimental data. The mixed MC sample (DIS+0.096*QE) consists of 36411 neutrino events with a vertex reconstructed in the emulsion target. The location efficiency is approximated by a parametrization that is a function of primary muon momentum and slope. In order to simulate Netscan procedure, realistic conditions of track densities need to be reproduced. This was achieved by merging the emulsion data of the simulated events with real Netscan data which do not have a reconstructed vertex but contain tracks which stop or pass through the Netscan volume, representing the real background. The combined data are passed through the same Netscan reconstruction and selection programs used for real data.

In order to test the reliability of the electronic detector simulation, we focus on the following quantities: vertex reconstruction, muon and hadron reconstruction efficiency and momentum distribution.

To check the behavior of the vertex reconstruction in MC, the main comparison is the track multiplicity. As seen from Figure 4.1 , the track multiplicity from primary vertex shows a reasonable agreement. The discrepancy in the first bin is mainly due to the lack in the simulated sample of the associated beam muons and of the ν interactions in a capillary test target placed in front of the CHORUS detector. In fact both these neglected components are mostly reconstructed as one track vertices in the first stack. The fraction of one track vertices are given

in Table 4.2.

The θ_μ, angle of the muon with respect to the beam direction, distribution is shown in Figure 4.4. The agreement between data and MC is reasonable, there is a small discrepancy at small θ. Two different explanations can be given: uncertainty in the event generator and clean detector simulation. The events for which the discrepancy is observed are characterized by low q^2. The DIS event generator at low q^2 has a sizeable uncertainty because it implies an extrapolation of the nucleon structure functions from high q^2 region where they are measured, to low q^2 region.

Table 4.2: The fraction of the single prong vertices in each stack for Mc and 1996-1997 data

Stack Number	1996	1997	MC
I	0.318 ± 0.005	0.323 ± 0.004	0.260 ± 0.005
II	0.225 ± 0.005	0.229 ± 0.004	0.185 ± 0.004
III	0.277 ± 0.005	0.288 ± 0.004	0.194 ± 0.004
IV	0.182 ± 0.004	0.195 ± 0.004	0.136 ± 0.003

The 4.2 shows the muon momentum distribution of data and MC events. The agreement of the data and simulated events is quite satisfactory until 30 GeV/c. There is a step after $P_\mu > 30 GeV/c$ in 1996 data; MC is higher than data. This discrepancy is due to a bug in the event location procedure. On the other hand, the agreement in 1997 data is quite satisfactory. A correction factor for 1996

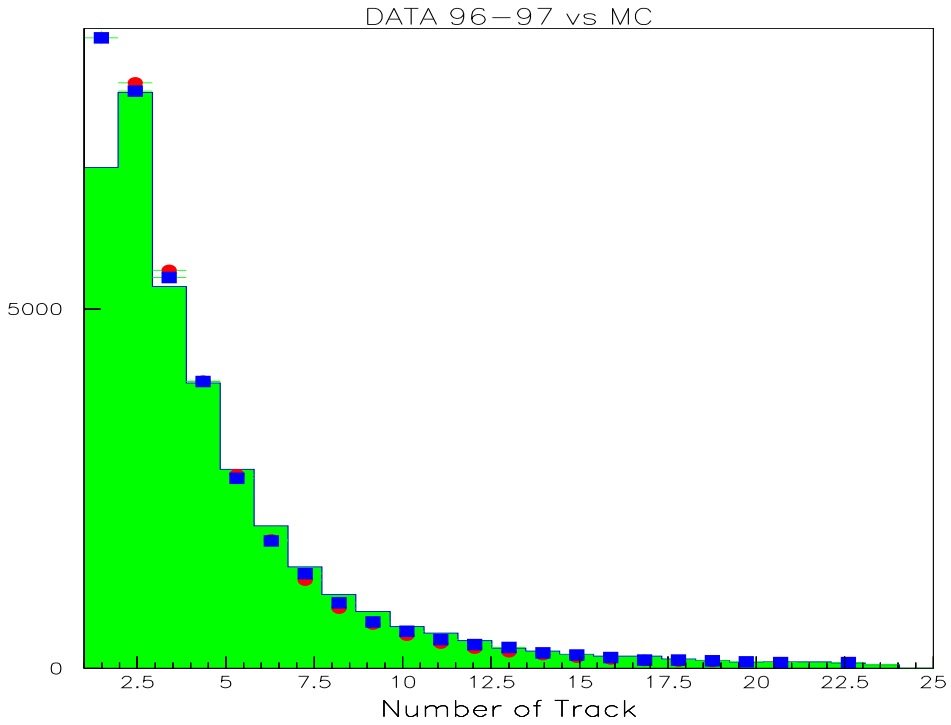

Figure 4.1: Track multiplicity distribution. Histogram for MC, dot for 1997 data, box for 1996 data.

data is evaluated from the measured ratio of 0.35 ± 0.02 between events with $P_\mu > 30GeV/c$ and $P_\mu < 30GeV/c$. This factor is found to be 1.02.

The calorimeter energy is shown in Figure 4.3, the Data and MC agree quite well. The only discrepancy can be seen at $E_{cal} \geq 80GeV$.

In order to check the reliability of the event generator, we also compared kinematical quantities:

- $E_{vis} = E_\mu + E_{had}$
- $Q^2 = 2E_\nu(E_\mu - P_\mu cos\Theta_\mu) - m_\mu^2 \approx 4E_\nu P_\mu sin^2\frac{\Theta_\mu}{2}$

- $x = \frac{Q^2}{2M_N E_{had}}$
- $y = \frac{E_{had}}{E_\nu}$
- $W^2 = M_N^2 - Q^2 + 2M_N E_{had}$

Here, E_{vis} is the visible energy, Q^2 is referred to as the momentum transfer, the variable Bjorken-x is the fraction of the nucleon energy processed by the struck quark, the variable Bjorken-y is the fraction of the available energy associated with the recoiling mass, and W^2 is the invariant mass squared.

Figure 4.5 shows the Q^2 distribution, the agreement between the DATA and the MC is quite good.

As shown in Figure 4.6, for the Bjorken-x, there is a good agreement between the DATA and MC.

Figure 4.7 shows the comparison of Bjorken y, the agreement between the DATA and the MC is reasonable. There is discrepancy in the last few bins. This is mainly due to uncertainty in the event generator.

Finally, Figure 4.8 shows W^2 distribution. There is a good agreement between the DATA and the MC.

4.7 Estimation of Number of Charged(Neutral)-Current Interactions

We have performed detailed DATA and MC comparisons for events originating in emulsion. In general the DATA and the MC agree well. Specially, the

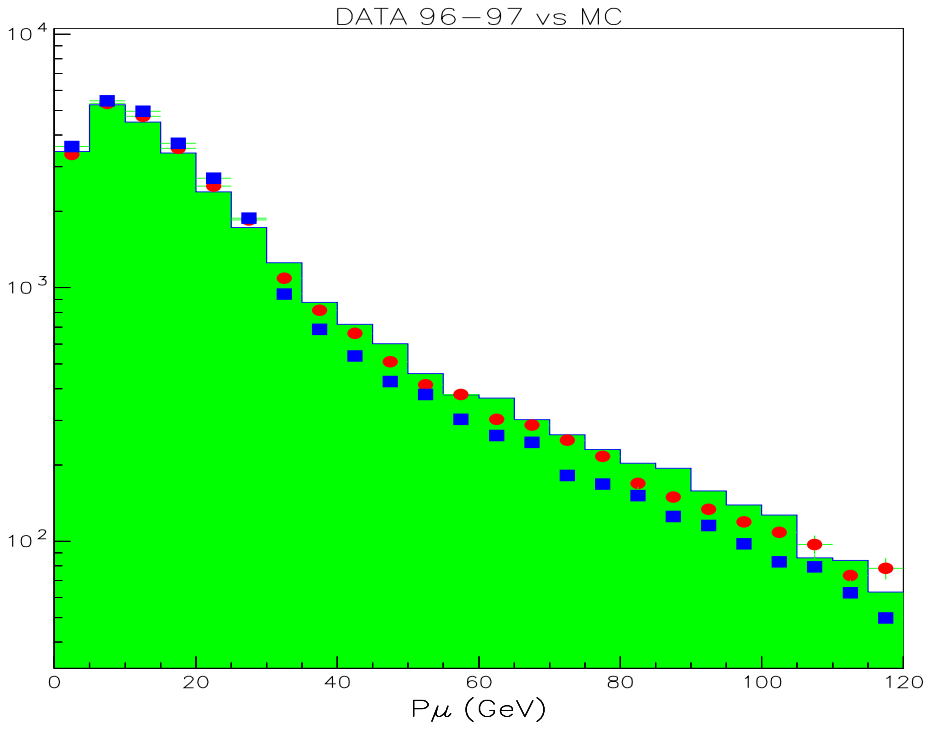

Figure 4.2: Muon momentum distribution. Histogram for MC, dot for 1997 data, box for 1996 data.

simulation of detector response is quite satisfactory. However, in some cases small discrepancies are observed. The discrepancy between the DATA and MC is within 10%. We also test simulation of events at the level of the event generator. The agreement between the DATA and the MC is satisfactory.

1μ sample contains mainly ν_μ CC interaction and a small contamination from ν_μ NC interaction and the 0μ sample mainly contains ν_μ NC interactions and a contamination from ν_μ CC interactions. The number of real NC ν_μ events is

$$N_{loc}^{NC\ 0\mu} = N_{loc}^{0\mu} - (N_{loc}^{1\mu} \times \frac{\varepsilon_{0\mu}^{CC}}{\varepsilon_{1\mu}^{CC}}) \tag{4.1}$$

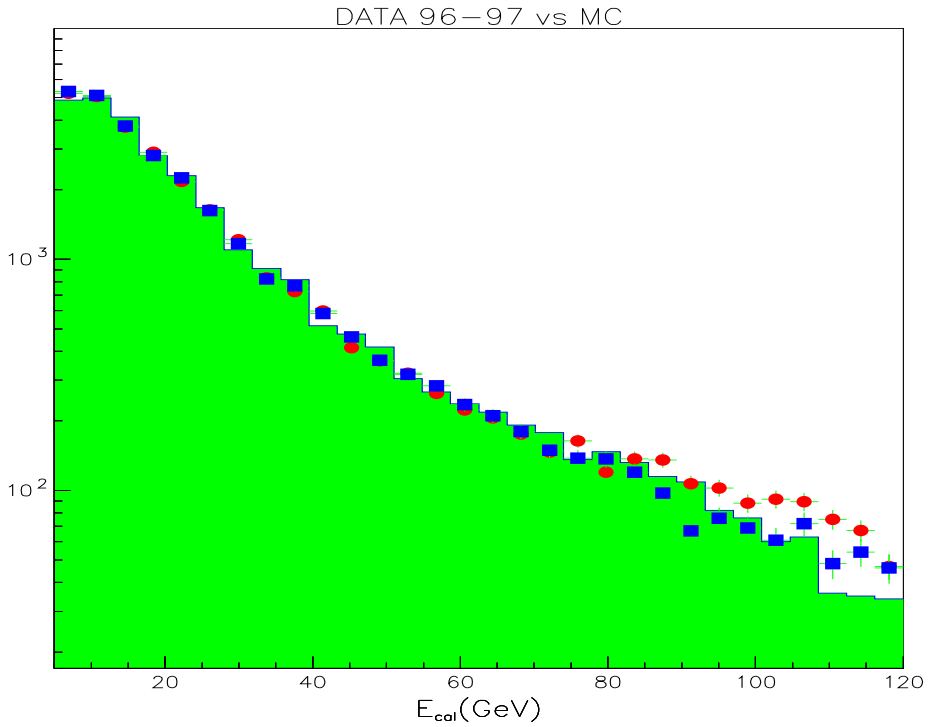

Figure 4.3: Total energy deposited in the calorimeter distribution. Histogram for MC, dot for 1997 data, box for 1996 data.

where $N_{loc}^{NC\ 0\mu}$: ν_μ NC interactions correctly seen as 0μ

$N_{loc}^{1\mu}$: ν_μ CC interactions wrongly seen as 0μ The contamination in 0μ sample is estimated to be 2134. The location efficiencies of NC DIS and CC ν_μ events are found to be 0.360 ± 0.003 and 0.027 ± 0.002 respectively.

In the estimation of $\frac{NC}{CC}$ratio, we have used only 1997 data. Since the scan back location strategy of 0μ sample was different in 1996. All 0μ events from 1996 data taking were searched and located in emulsion. For 1997 data, only events which have at least one track with DT hits were scanned in emulsion. Therefore

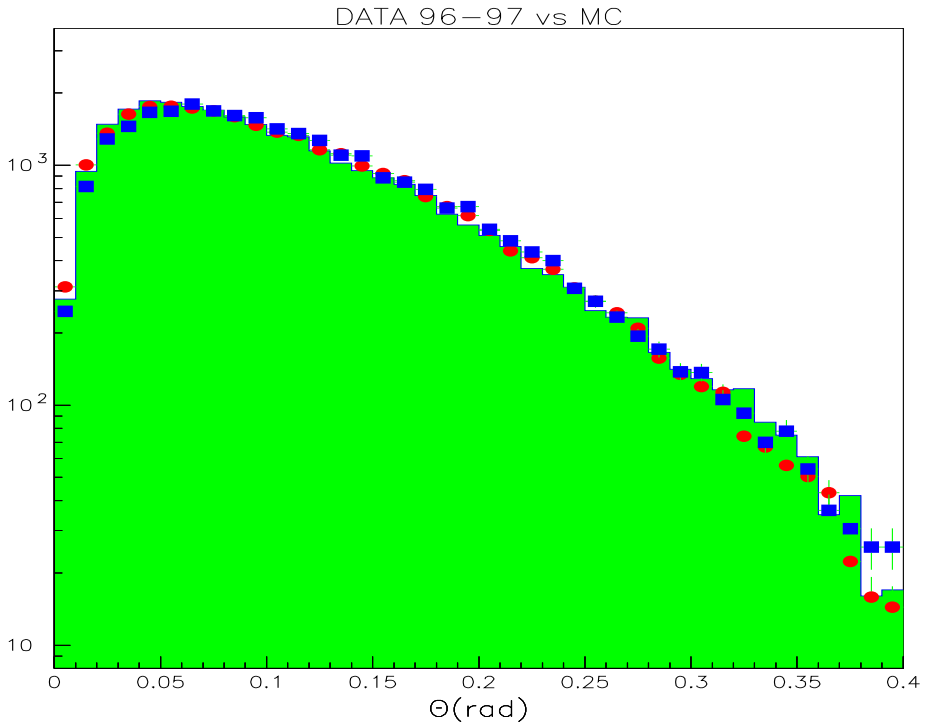

Figure 4.4: Muon slope distribution. Histogram for MC, dot for 1997 data, box for 1996 data.

$\frac{0\mu}{1\mu}$ ratio is different for 1996 data, it is greater than 1997 data.

After subtracting the contamination and correcting for efficiency, we obtain $\frac{NC_{dis}}{CC} = 0.320 \pm 0.003$. In order to compare the our result with the previous measurements we also evaluate the ratio of NC DIS to CC DIS ν_μ interactions to be $\frac{NC_{dis}}{CC_{dis}} = 0.350 \pm 0.003$ by taking QE=DIS$\times$0.096 [**?**]. Our result is consistent with previous measurements, as given in Table 4.4.

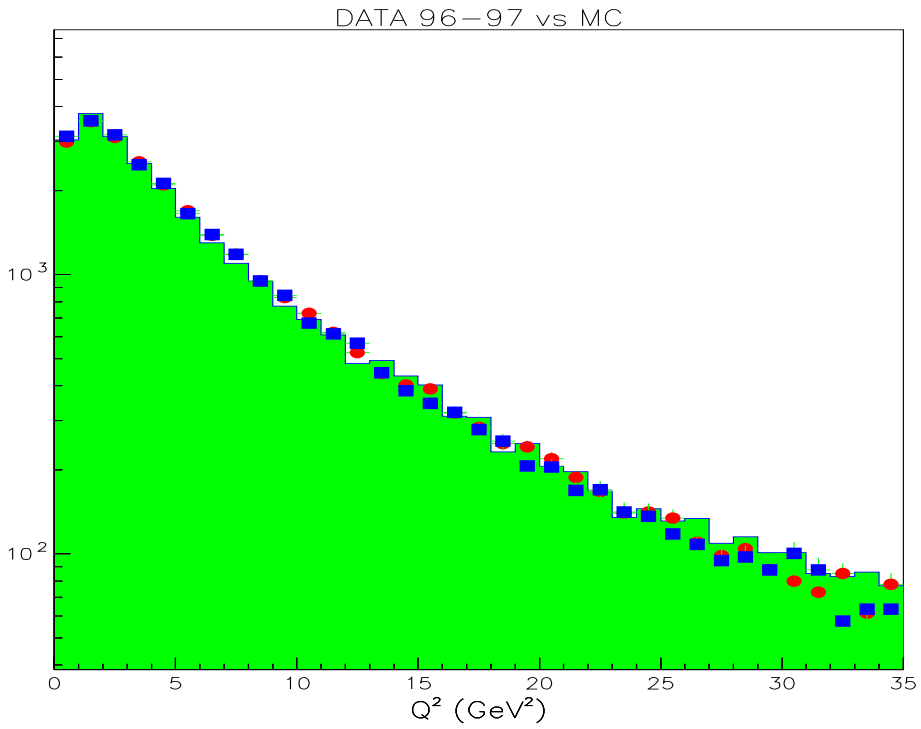

Figure 4.5: Q^2 distribution. Histogram for MC, dot for 1997 data, box for 1996 data.

Table 4.3: MC sample used in analysis

Selection Criteria	In Emulsion
CC DIS in emulsion	27729
CC DIS located	9588
QE in emulsion	5385
QE located	2818
NC DIS in emulsion	37995
NC DIS located	5527

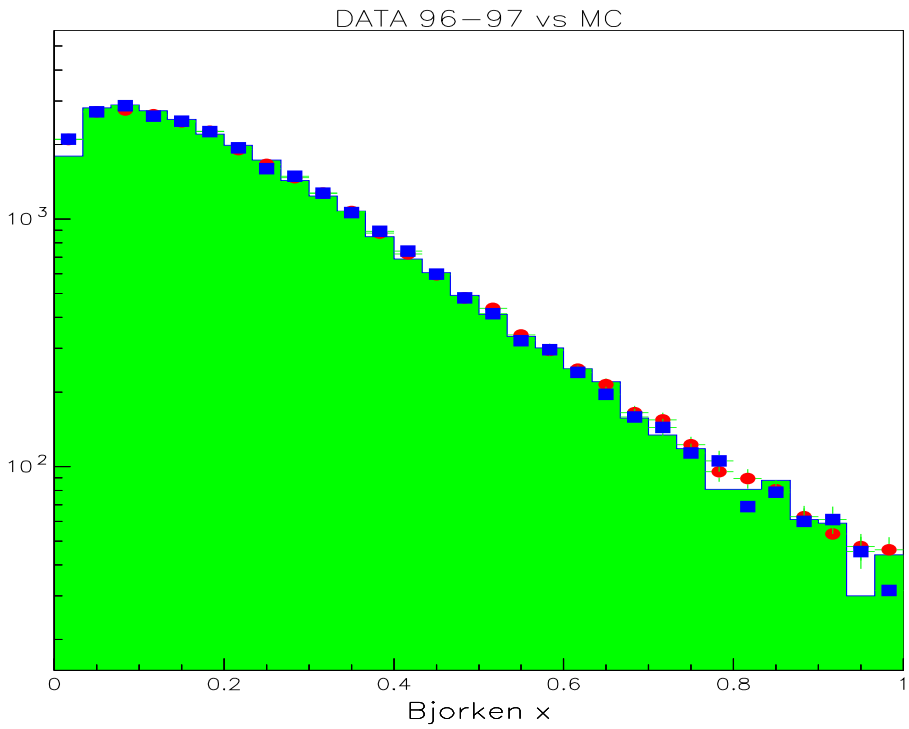

Figure 4.6: Bjorken-x distribution. Histogram for MC, dot for 1997 data, box for 1996 data.

Table 4.4: $\frac{NC}{CC}$, measured by other experiments

Experiment	$\frac{NC_{dis}}{CC_{dis}}$
CDHS[42]	0.307 ± 0.003
CHARM[43]	0.309 ± 0.003
CCFR[44]	0.415 ± 0.001
CHORUS	0.327 ± 0.003

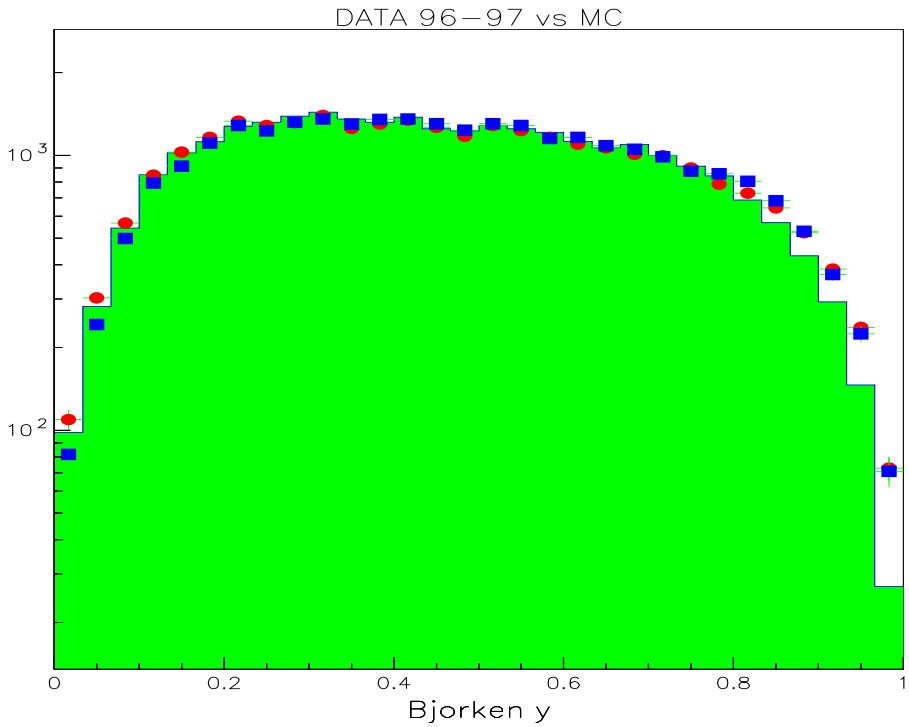

Figure 4.7: Bjorken-y distribution. Histogram for MC, dot for 1997 data, box for 1996 data.

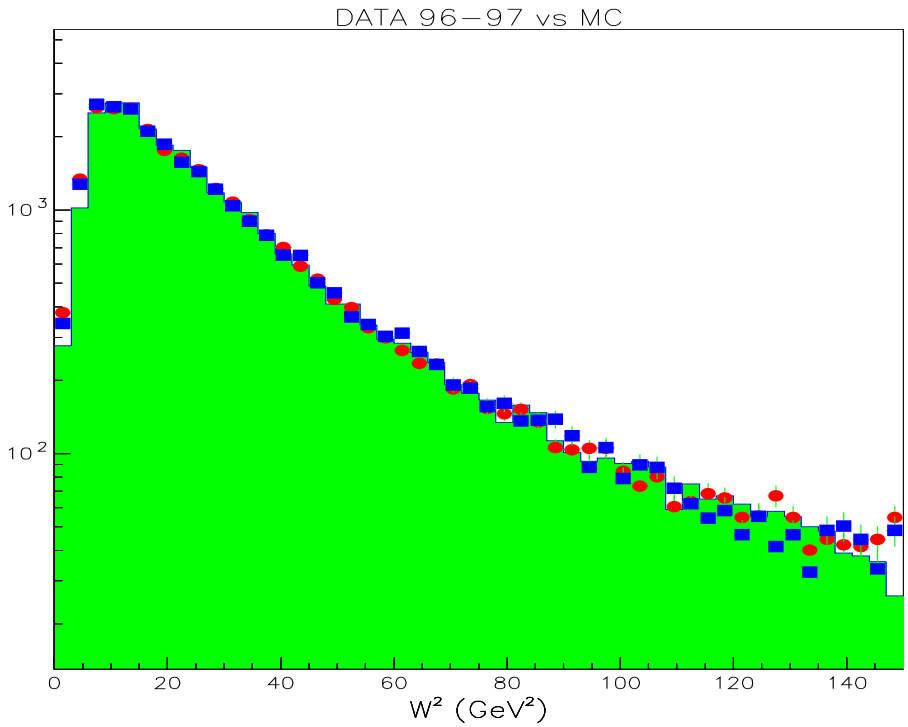

Figure 4.8: W^2 distribution. Histogram for MC, dot for 1997 data, box for 1996 data.

CHAPTER 5

ASSOCIATED CHARM PRODUCTION IN NEUTRINO INTERACTIONS

The associated charm production in neutrino nucleon scattering is a very rare process and therefore difficult to measure. The charm pair originates from two different processes: one is the so-called boson-gluon fusion mechanism in the neutral current interactions and other one is the gluon bremsstrahlung in charged current interactions.

All the previous results on associated charm production in neutrino interactions were extracted from multi-muon samples with a large background of non prompt muons. In the CHORUS experiment a different search in the nuclear emulsion was carried out, practically background free. The search is based on the visual observation of two decay vertices, taking advantage of the submicrometric position resolution of the nuclear emulsions exposed in the CHORUS experiment to the CERN SPS neutrino beam.

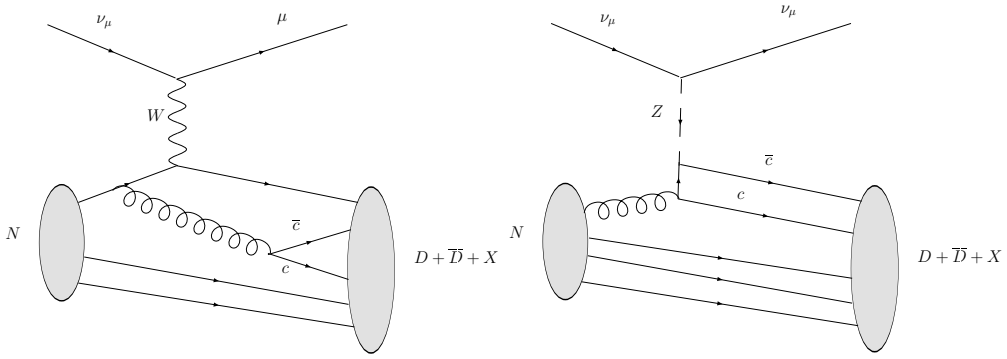

Figure 5.1: Associated charm production in ν_μ CC(left) and NC(right) interaction.

5.1 Selection of Double Charm Decays

In total about 130,000 ν_μ events have been located in emulsion with procedure described in Chapter 3.

To select interesting decay topologies while preserving a good efficiency for decay finding, the following selection criteria are applied [34] to 0μ and 1μ [1] samples:

- Define vertices on the basis of the minimum distance between tracks and define as primary the one with at least one track matching with tracks reconstructed by the fiber tracker system.
- Select events with both primary and decay vertices reconstructed.
- Select tracks originating from the primary vertex and stopping in the Netscan

[1] The selection criteria applied to the 1μ sample are similar to those applied to the the 0μ sample. The main difference is that, given the fact that the muon is usually more efficiently reconstructed by the electronic detectors as well as in the emulsions due to its higher momentum, a special weight is given to the muon track by the algorithm used for the primary vertex reconstruction.

volume, thus identifying a possible secondary vertex.

- Select tracks originating in the same plate as the primary vertex and with an impact parameter to the primary vertex larger than the value determined on the basis of resolution.

- Require for the above tracks that the direction measured in emulsion matches the one reconstructed by the fiber tracker system.

From the sample of 26,621 (99,245) scanned and analyzed 0μ (1μ) events, the selection criteria select 717(2816) events which are then visually inspected to confirm the decay topology. A secondary vertex is accepted as decay if the number of prongs is consistent with charge conservation and if no other activity (Auger electron or "blob") is observed. Moreover, to avoid a visual inspection inefficiency, decays into a single charged particle, *kink topology*, are accepted only if the angle between parent and daughter is greater than 50 mrad and the flight length (distance between primary vertex and decay vertices) is greater than 25μm. A secondary vertex is accepted as decay if the number of prongs is consistent with charge conservation. The observable decay topologies are classified as odd-prong and even-prong decays. These are denoted as V2, V4, V6 for neutral and C1, C3, C5 for charged decays. The results are given in Table 5.1 for 0 μ sample and in Table 5.2 for 1μ sample.

The rejected sample mainly consist of hadronic interactions, γ conversions and

of low momentum tracks. After topological confirmation of decays further kinematical selection is applied in order to reduce the background coming from strange particles. For the kink topology a selection $P_T > 0.250 GeV/c$ on the transverse momentum of the decay particle with respect to the parent direction is applied, in order to reject C1 decays of strange particles. For the V2 decay topology a selection $\phi > 0.010$rad,where $\phi$is the angle between the parent direction and the plane formed by daughter particles, is applied. This selection eliminates the two body decay of strange particles. the effects of these kinematical cuts are included in finding the Netscan efficiencies.

There are four events, three in 0μ sample and one in 1μ sample which satisfied the selection criteria above. The sketch of each event in emulsion is shown in Figures 5.2, 5.3, 5.4 and 5.5. Details of each double charm event is given in Tables 5.1 and 5.2.

Table 5.1: Details of NC double charm events

Event id	Decay topology	# of track	L_{Flight} (μm)	P_T (GeV/c)	ϕ (mrad)
8132-12312	V2	1	63	-	24.2
	V2	1	977	-	36
7692-5575	C1	2	426	0.32	179
	V2	2	224	-	14.9
7739-3952	C3	6	426	-	1
	V4	6	884	-	1

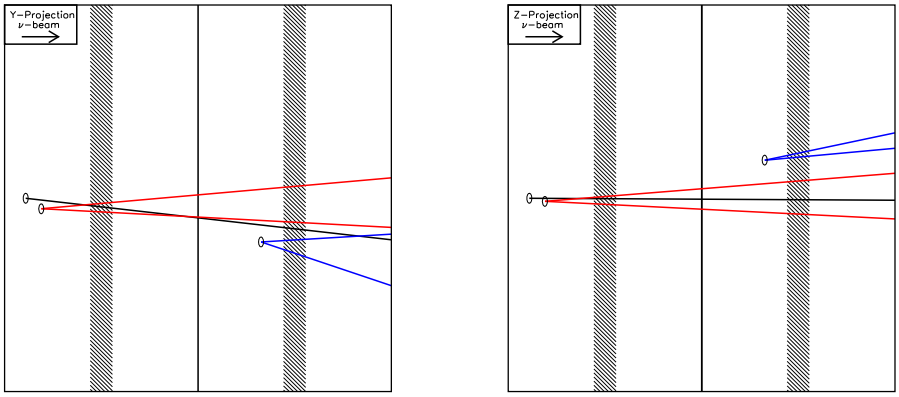

Figure 5.2: Sketch of candidate $c\bar{c}$ NC event (8132-12312) Y (Left), and Z (Right) projection.

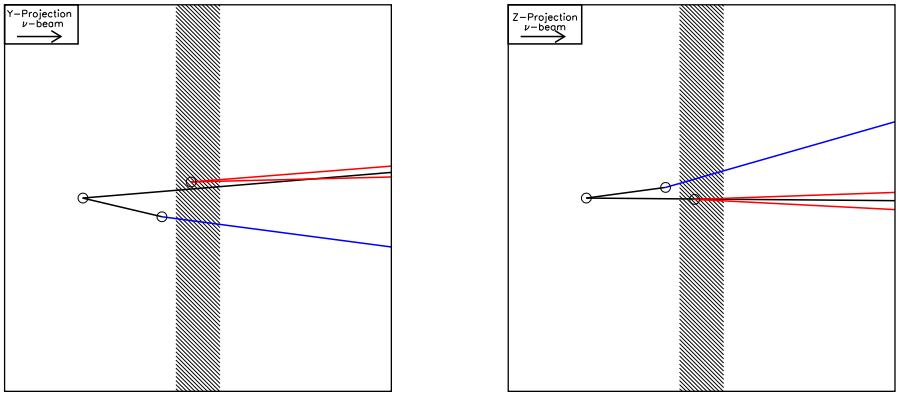

Figure 5.3: Sketch of candidate $c\bar{c}$ NC event (7692-5575) Y (Left), and Z (Right) projection.

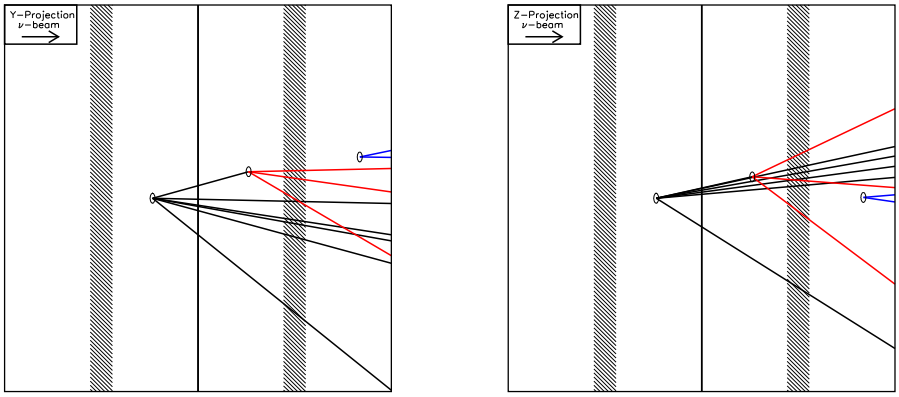

Figure 5.4: Sketch of candidate $c\bar{c}$ NC event (7739-3952) Y (Left), and Z (Right) projection.

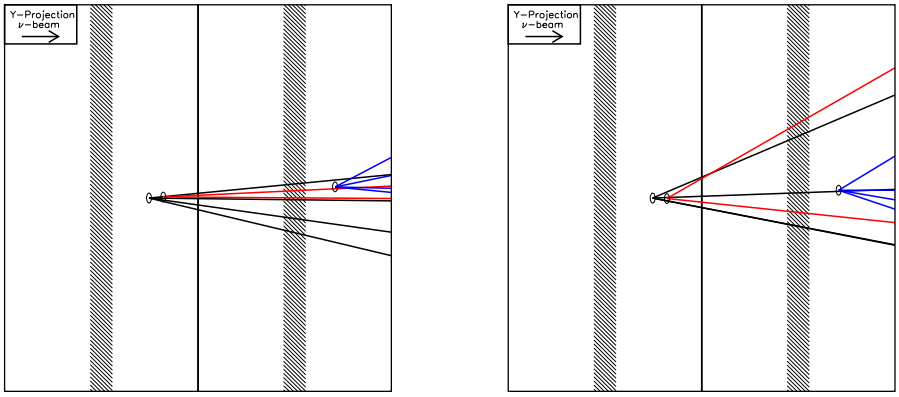

Figure 5.5: Sketch of candidate $c\bar{c}$ CC event (7904-4944) Y (Left), and Z (Right) projection.

Table 5.2: Details of CC double charm events

Event id	Decay topology	# of track	L_{Flight} (μm)	P_T (GeV/c)	ϕ (mrad)
7904-4999	V2	4	58	-	12.8
	V4	4	313	-	1

Table 5.3: Results of the visual inspection in the selected 0μ sample.

Charm candidates		Rejected events	
Topology	Events	Category	Events
V2	145	low momentum	72
V4	43	$h^{\pm}$ int.	110
C1	80	h^0 int.	4
C3	75	γ- conversion	36
C5	4	resolution tail	108
V2+V2	1	accidentally found	37
C1+V2	1		
C3+V4	1		
Total	350		367

5.2 Efficiency Estimation

The HERWIG event generator is used to generate large samples of neutrino interactions [45]. Efficiencies and backgrounds were evaluated with a simulation of the detector based on GEANT3. In order to evaluate the Netscan procedure efficiency a realistic conditions of track densities must be reproduced. This was achieved by merging the emulsion data of the simulated events with real Netscan data representing the real background [33]. The combined data are

Table 5.4: Results of the visual inspection in the selected 1μ sample.

Charm candidates		Rejected events	
Topology	Events	Topology	Events
V2	841	low momentum	140
V4	230	$h^{\pm}$ int.	258
V6	3	h^0 int.	69
C1	462	γ- conversion	101
C3	501	resolution tail	149
C5	23	accidentally found	36
C1+C3	1		
C1+V2	1		
V2+V4	1		
Total	2063		753

passed through the same Netscan reconstruction and selection programs as used for real data.

The selection efficiencies are given in Table5.5. The ratio of reconstruction and location efficiency of events with $c\bar{c}$ in ν_μ CC (NC) events to that of all ν_μ CC (NC) events is found to be $50.6 \pm 1.8\%$ ($49.6 \pm 2.2\%$). The low reconstruction and location efficiency of $c\bar{c}$ events is due to large hadronic activity in the electronic detector.

Table 5.5: MC selection efficiencies

Sample	Netscan efficiency
NC	12.8 ± 0.6 %
CC	5.5 ± 0.6 %

5.3 Background Estimation

A double charm event is topologically indistinguishable from a single charm event with a primary non-charmed hadron which undergoes either a decay or an interaction without any visible recoil of the nuclei. The decay length makes negligible contribution for decays of other non-charmed hadrons like kaons and pions.

The non-charmed hadron produced in a single charm event can interact with a nucleus. The corresponding interaction length is very large, ranging from a few meters for the single prong interactions to several hundred meters for the multi-prong ones. A simulation of these processes using FLUKA [20] has been carried out and the interaction lengths for the different processes have been obtained. A number of interactions in emulsion has been collected by CHORUS in studies of charm decays. This allows experimental cross checks of the calculations. An overall background of 0.79 ± 0.10 events is expected in the CC interactions.

The only difference with respect to the CC search is in the muon misidentification in single charm events. An overall background of 0.12 ± 0.02 events is expected.

Table 5.6: Background sources and the corresponding event yields in the CC search.

Primary interaction	secondary vertex	event yield
$\nu_\mu N \to \mu^- c\Sigma^\pm X$	$\Sigma^\pm \to$ 1 prong	0.002 ± 0.001
$\nu_\mu N \to \mu^- c h^\pm X$	$h^\pm$ white kink	0.08 ± 0.02
$\nu_\mu N \to \mu^- c h^\pm X$	$h^\pm$ white trident	0.06 ± 0.02
$\nu_\mu N \to \mu^- c h^\pm X$	$h^\pm$ white C5	0.024 ± 0.005
$\nu_\mu N \to \mu^- c h^0 X$	h^0 white V2	0.01 ± 0.01
$\nu_\mu N \to \mu^- c h^0 X$	h^0 white V4	0.006 ± 0.006
Overall		0.18 ± 0.03

Table 5.7: Background sources and the corresponding event yields in the NC search.

Primary interaction	secondary vertex	event yield
$\nu_\mu N \to \not{\mu}^- c\Sigma^\pm X$	$\Sigma^\pm \to$ 1 prong	0.0003 ± 0.0001
$\nu_\mu N \to \not{\mu}^- c h^\pm X$	$h^\pm$ white kink	0.011 ± 0.002
$\nu_\mu N \to \not{\mu}^- c h^\pm X$	$h^\pm$ white trident	0.010 ± 0.002
$\nu_\mu N \to \not{\mu}^- c h^\pm X$	$h^\pm$ white C5	0.0038 ± 0.0007
$\nu_\mu N \to \not{\mu}^- c h^0 X$	h^0 white V2	0.001 ± 0.001
$\nu_\mu N \to \not{\mu}^- c h^0 X$	h^0 white V4	0.0005 ± 0.0005
Overall		0.025 ± 0.003

5.4 Estimation of Associated Charm Production Rate

In order to estimate associated charm production rate in ν_μ interactions, an additional weight factor needs to be applied to 1μ events with $P_\mu > 30$ GeV/c, since a small fraction of this category was not located and analyzed. This factor was evaluated from the measured ratio 0.305 ± 0.002 of 1μ events with $P_\mu > 30$ GeV/c to those with $P_\mu < 30$ GeV/c; it was found to be 1.02. In order to evaluate the real number of ν_μ NC, we have used our measurement of the fraction:

0.320±0.003 between NC and CC ν_μ interactions.

After background subtraction and efficiency correction we estimate the average rate of NC associated charm production at the average neutrino energy 27 GeV as

$$\frac{\sigma(c\bar{c}\nu_\mu)}{\sigma_{NC}} = (3.37^{+3.06}_{-2.51}(stat.) \pm 0.51(syst.)) \times 10^{-3}.$$

The statistical error was derived using 68% confidence interval in the unified approach for the analysis of small signals in the presence of background [48]. We have accounted for a systematic uncertainty of 15% coming from efficiency estimation by Monte Carlo modeling. The measured cross-section ratio in NC interactions is consistent with the E531 [20] measurement:

$$\frac{\sigma(c\bar{c}\nu_\mu)}{\sigma_{NC}} = (13^{+31}_{-11}) \times 10^{-4}$$

.

With the observation of one double charm event in CC interactions, we obtain an upper limit at 90% CL [48] of

$$\frac{\sigma(c\bar{c}\mu^-)}{\sigma_{CC}} < 9.69 \times 10^{-4}.$$

CHAPTER 6

RESULTS AND DISCUSSION

The CHORUS experiment was designed to search for $\nu_\mu \rightarrow \nu_\tau$ oscillations through direct observation of ν_τ CC interactions in the emulsion target. During the exposure periods of 1994 and 1997, the emulsion target had been exposed to the neutrino beam for an integrated intensity of 5.06×10^{19} protons on target. The improvement of the automatic scanning system in the experiment allows also an efficient search for charmed particles with high statistics.

In this study, we have done detailed DATA/MC comparisons of events located in emulsion. The agreement between DATA and MC sample is satisfactory. There are small discrepancies, which are mainly due to uncertainties in the event generator and too clean simulation of detector response.

After subtracting contamination and correcting for efficiencies, the ratio of DIS NC ν_μ to DIS CC ν_μ interactions was measured to be $\frac{NC_{dis}}{CC_{dis}} = 0.350 \pm 0.003$. This measurement is consistent with the previous measurements.

Based on the observed three double charm events in 0μ we have measured the average rate of NC associated charm production at the average neutrino energy

27 GeV as

$$\frac{\sigma(c\bar{c}\nu_\mu)}{\sigma_{NC}} = (3.37^{+3.06}_{-2.51}(stat.) \pm 0.51(syst.)) \times 10^{-3}. \tag{6.1}$$

With the observation of one double charm event in CC interactions, we obtain an upper limit at 90 %C.L. of

$$\frac{\sigma(c\bar{c}\mu^-)}{\sigma_{CC}} < 9.69 \times 10^{-4}. \tag{6.2}$$

REFERENCES

[1] C.W.Kim and A.Pevsner, *Neutrino in Physics and Astrophysics*, Harwood academic Publishers, Pennsylvania, 1993.

[2] R.N.Mohapatra and P.B.Pal,*Massive Neutrinos in Physics and Astrophysics*, River Edge, N.J. World Scientific, 2004.

[3] Von Bayer, O. Hahn, and L. Meitner, Physik. Zeits. **14**, 873 (1913).

[4] E. Rutherford, Philosophical Magazine Series 6, **21** 1911, 669-688

[5] Chadwick, J., Verh. Deutsch. Phys. Ges., **16**, 383 (1914).

[6] J. Chadwick, Proc. Roy. Soc. **A136** 692 (1932).

[7] E Fermi Z. Physik 88-161 (1934)

[8] R. H. Dalitz, Rudolf Ernst Peierls *Selected Scientific Papers of Sir Rudolf Peierls: With Commentary*, World Scientific Series in 20th century,1997.

[9] F.Reines and C.L. Cowan, Phys. Rev. Lett. **92**,830 (1953).

[10] J.Steinberger et al., Phys. Rev. Lett. **109**,1015 (1962).

[11] M.Perl et al. Phys. Rev. Lett. **35**,1489 (1975).

[12] B.Lundberg (DONUT coll.), to appear on the Proc. of the XIX. Int. Conf. on Neutrino Physics and Astrophysics,(2000).

[13] N.Cabibbo, Phys. Rev. Lett. **10**,531 (1963).

[14] M.Kobayashi and T.Maskawa, Prog. Theor. Phys. **49**,652 (1973).

[15] A. Pich, FTUV/95-19; IFIC/95-19, hep-ph/9505231 **v1** 1995

[16] David J. Gross, Nucl.Phys.Proc.Suppl. **74** (1999) 426-446, hep-th/9809060

[17] M. Cohen and R. P. Feynman Phys. Rev. 107, **13-24** (1957)

[18] Bjorken, James and Drell, Sidney. "Relativistic Quantum Mechanics", McGraw-Hill (1964). ISBN 0-07-005493-2

[19] L. Maiani, Cambridge Monogr. Part. Phys. Nucl. Phys. Cosml. *1*, 278, (1991).

[20] N.Ushida et. al.,E531 Collaboration Phys. Lett. **B, 206**, 375 (1988).

[21] F.Dydak et. al.,CDHS coll. Phys. Lett. **B,134**,281 (1984).

[22] A.Rubia, Proceedings of the Third Workshop on Tau Lepton Physics, Montreux, Switzerland 1994 Nucl. Phys. **B 40**,85 (1995).

[23] A.O.Bazarko, CCFR collaboration hep-ex/9406007 (1994).

[24] S.Glashow, Nucl. Phys. Rev. **22**,579 (1961).

[25] A.Salam, Phys. Lett. **13**, 168 (1964).

[26] S.Weinberg, Phys. Rev. Lett. **19**, 1264 (1967).

[27] R. M. Barnett,Phys. Rev. Lett. **36**, 1163 (1976).

[28] R. M. Barnett,Phys. Rev. **D 14**, 70 (1976).

[29] E. Eskut et. al., Nucl. Instrum. and Meth. **A 401**, 7 (1997).

[30] G. Acquistapace et. al. The West Area Neutrino Facility for CHORUS and NOMAD experiments:1994-1997 operation. CERN-ECP-95-014.

[31] F. Bergsma et al., NIM. textbfA357 (1995) 243

[32] U. Köse, M. Sc. Thesis, Middle East Technical University (2002).

[33] M. Güler, O. Sato, CHORUS internal Note 2000017 (2002).

[34] M. Guler Phd Thesis, METU, Ankara, CERN-THESIS-2002-027 (2000).

[35] S. Sorrentino, CERN-PPE/98-005, (1998).

[36] A. Fasco et al., SARE-3 Workshop, KEK Report Proceedings 97-5, p.32 (1997).

[37] G. Ingelman et al., DESY 96-057, (1996).

[38] M. Gluck, E.Reya and A. Vogt, Z. Phys.**C67** (1995) 433-448.

[39] P. Zucchelli and I. Tsukernman, CHORUS Internal Note 2000007.

[40] P. Zucchelli, PhD Thesis, Univ. of Ferrara, Italy, 1992/1994.

[41] S. Ricciardi, CHORUS Internal Note 97001.

[42] CDHS Collab., A. Blondel et al, Z. Phys. **C45** (1990) 361.

[43] CHARM Collab., J. L. Allaby et al, Z. Phys. **C36** (1987) 611.

[44] CCFR Collab., K. S. McFarland et al, Eur. Phys. J. **C41** (1998) 501

[45] HERWIG 6.5 G. Corcella et. al.,JHEP 0101 (2001) 010 hep-ph/0210213.

[46] GEANT 3.21, CERN program library long write up W5013

[47] CCFR Collaboration Eur. Phys. J. *C1*, (1998).

[48] G. J. Feldman and R. D. Cousins, Phys. Rev. *D57*, 3873 (1998).

[49] NuTeV Collaboration, Phys. Rev. *D64*, 012002 (2001), Int. J. Mod. Phys. A16S1B, 766 (2001).